the plant journal

SEB SOCIETY FOR EXPERIMENTAL BIOLOGY

The Plant Journal (2024) **119,** 2885–2903 doi: 10.1111/tpj.16959

An incoherent feed-forward loop involving bHLH transcription factors, Auxin and CYCLIN-Ds regulates style radial symmetry establishment in Arabidopsis

William Tasker-Brown[1,†], Samuel W. H. Koh[2,‡], Nicola Trozzi[2,3], Kestrel A. Maio[2], Iqra Jamil[2], Yuxiang Jiang[2,§], Mateusz Majda[3,¶], Richard S. Smith[3] and Laila Moubayidin[1,2,*]

[1]*Department of Crop Genetics, John Innes Centre, Norwich, Norfolk, UK,*
[2]*Department of Cell and Developmental Biology, John Innes Centre, Norwich, Norfolk, UK,*
[3]*Department of Computational and Systems Biology, John Innes Centre, Norwich, Norfolk, UK*

Received 7 February 2024; revised 18 June 2024; accepted 23 July 2024; published online 9 August 2024.
*For correspondence (e-mail laila.moubayidin@jic.ac.uk).
[†]Present address: Tropic Biosciences Ltd, Norwich Research Park Innovation Centre, Norwich NR4 7GJ, UK
[‡]Present address: Laboratory of Biochemistry, Wageningen University, Wageningen, The Netherlands
[§]Present address: Institute of Biology Leiden, Leiden University, Leiden, The Netherlands
[¶]Present address: Department of Plant Molecular Biology, University of Lausanne, Lausanne, Switzerland

SUMMARY

The bilateral-to-radial symmetry transition occurring during the development of the *Arabidopsis thaliana* female reproductive organ (gynoecium) is a crucial biological process linked to plant fertilization and seed production. Despite its significance, the cellular mechanisms governing the establishment and breaking of radial symmetry at the gynoecium apex (style) remain unknown. To fill this gap, we employed quantitative confocal imaging coupled with MorphoGraphX analysis, *in vivo* and *in vitro* transcriptional experiments, and genetic analysis encompassing mutants in two bHLH transcription factors necessary and sufficient to promote transition to radial symmetry, SPATULA (SPT) and INDEHISCENT (IND). Here, we show that defects in style morphogenesis correlate with defects in cell-division orientation and rate. We showed that the SPT-mediated accumulation of auxin in the medial-apical cells undergoing symmetry transition is required to maintain cell-division-oriented perpendicular to the direction of organ growth (anticlinal, transversal cell division). In addition, SPT and IND promote the expression of specific core cell-cycle regulators, CYCLIN-D1;1 (CYC-D1;1) and CYC-D3;3, to support progression through the G1 phase of the cell cycle. This transcriptional regulation is repressed by auxin, thus forming an incoherent feed-forward loop mechanism. We propose that this mechanism fine-tunes cell division rate and orientation with the morphogenic signal provided by auxin, during patterning of radial symmetry at the style.

Keywords: style development, radial symmetry, cell-division orientation, G1-phase progression, incoherent feed-forward loop, CYCLIN-D1;1, CYCLIN-D3;3, auxin, gynoecium, transcriptional regulation.

INTRODUCTION

A fundamental aspect for the correct morphogenesis of multicellular organisms is the establishment and breaking of organ symmetry during development. Bilateral, biradial and radial symmetry are the most common symmetry types displayed by biological structures, in which a multicellular body can be divided by one, two and three or more planes of symmetry, respectively (Moubayidin & Østergaard, 2015). This fundamental feature is at the basis of how tissues and organs develop and function, and how multicellular bodies are patterned into their three-dimensional shapes, both during embryogenesis and beyond (Genikhovich & Technau, 2017). While in metazoan symmetry-breaking events, polarity cues and directional cell migration contribute profoundly to morphogenesis (Davison et al., 2016; Erzberger et al., 2020), plant cells are largely immobile due to a rigid cell wall, meaning organ symmetry in plants is mainly controlled at the level of a dynamic equilibria between cell division and cell differentiation. Fine-tuning these equilibria means controlling the rate of cell division, its timing and orientation as well as how cells expand and differentiate during patterning and growth (D'Ario et al., 2021; Dello Ioio et al., 2008; Facette et al., 2018).

Although pivotal for organ function, the molecular and cellular bases presiding over the foundation of

symmetric shapes during plant organogenesis are still poorly understood. We previously showed that the female reproductive structure of *Arabidopsis thaliana* is an ideal model to tackle how organ symmetry is controlled because it undergoes a rare type of symmetry transition during its development: from bilateral symmetry in the ovary (where seeds develop) to radial symmetry at its apical end in a structure called the style (important for fertilization) (Figure 1A; Moubayidin & Østergaard, 2014).

The triggering event of this symmetry transition is initiated in specific medial-apical cells of the developing organ and requires a switch in polarity cues (Moubayidin & Østergaard, 2014). In particular, the morphogenetic signal provided by the plant hormone auxin (Sabatini et al., 1999) accumulates in those medial-apical cells undergoing the symmetry transition thanks to an unusual apolar distribution of its transporters (the PIN efflux carriers) at the plasma membrane (Friml et al., 2004; Moubayidin & Østergaard, 2014). Two key bHLH transcription factors, SPATULA (SPT) (Heisler et al., 2001) and INDEHISCENT (IND) (Liljegren et al., 2004), synergistically control the apolar distribution of PINs at the medial-apical cells (Moubayidin & Østergaard, 2014). Accordingly, loss-of-function mutants in these transcription factors fail to accumulate auxin in a 4-foci, biradial stage, and thus do not form a solid radial style: there is a break in symmetry, which manifests as a 'split-style' phenotype, visible as a cleft in the apical region (Figure 1A–D; Moubayidin & Østergaard, 2014). A similar split-style phenotype was also observed when polarization of PIN1 was impaired at the style region (via employing a phospho-mimic PIN1 mutant version), which led to a failure to accumulate auxin in the medial-apical cells where the break in radial symmetry is displayed (Moubayidin & Østergaard, 2014).

Thus, a radially symmetric pattern of PIN distribution at the cellular level correlates with radial symmetry at the organ level, scaling up symmetry from cells to organs. This raises the possibility that a cell-autonomous signal, for example auxin cellular levels, provides rules of cell division and growth necessary for radial symmetry establishment at the gynoecium apex and suggests a spatial–temporal genetic orchestration of organ patterning to ultimately fuse the two lateral carpels at the apical-medial region. This is in line with clonal analysis of wild-type (WT) gynoecia coupled with predictive mathematical modelling showing that growth at the style region is anisotropic, with more growth in the apical-basal direction, consistent with divisions oriented in the anticlinal (transversal) direction and cell expansion along the apical-basal direction (Eldridge et al., 2016; Gómez-Felipe et al., 2024).

Division plane orientation in plants is established before mitosis and must be maintained throughout mitosis and cytokinesis (Facette et al., 2018). This process is often thought to occur when the preprophase band (PPB) forms in the G2 phase of the cell cycle (Facette et al., 2018; Spinner et al., 2013), although the current scenario assigns the PPB a role in adding robustness to the selection of the right division angle, rather than being a key determinant of cell-division orientation *per se* (Schaefer et al., 2017). Thus, the coordination between cell division rate and orientation has been proposed to facilitate division plane determination in proliferating tissues, such as in the root meristem (Costa, 2017). This scenario is consistent with a requirement for a robust placement of cell division in the medial-apical cells, where auxin signaling accumulates (Moubayidin & Østergaard, 2014), to underpin the final fusion of the marginal tissue of the style. Thus, we hypothesize that there must be a tight regulation of cell division, both in orientation and rate, at the apical end of the gynoecium, orchestrated by SPT and IND.

Despite the fundamental and practical importance of symmetry establishment and transition at the gynoecium apex, the cellular basis of radial style morphogenesis is still not understood. Because organ morphogenesis depends on mechanical, genetic and environmental cues, growth and cell-division mechanisms are tightly connected. Our work provides genetic, molecular and cellular basis that link cell-division players and mechanisms to radialization of the Arabidopsis style. By means of quantitative confocal analysis, genetic experiments, *in vivo* and *in vitro* transcriptional analyses, here we show that an incoherent feed-forward loop (I-FFL), orchestrated upstream by SPT and IND, controls progression in G1-phase of the cell cycle via transcriptional regulation of two cell-cycle regulators, CYCLIN-D1;1 (CYC-D1;1) and CYC-D3;3 (Collins et al., 2012; Forzani et al., 2014). Our data show that SPT and IND control the rate of cell division in G1 by promoting the expression of *CYC-D1;1* and *CYC-D3;3*, and this positive control is, at least for IND, direct. In addition, SPT activity and auxin accumulation is important to maintain cell division in the transversal, anticlinal orientation, at the apical-medial domain. Auxin, whose accumulation is promoted upstream by SPT and IND, plays a negative effect on *CYC-D1;1* and *CYC-D3;3* expression, switching off their transcriptional regulation. This regulatory loop could presumably coordinate orientation of cell division with the rate and progression through the cell cycle, specifically in the auxin-responsive cells. Altogether, we propose a molecular and genetic mechanism underpinning the cellular behavior at the apical-medial region of the gynoecium apex as it undergoes a bilateral-to-radial symmetry transition.

RESULTS

Bilaterally symmetric styles display a switch in cell-division orientation

A close observation by scanning electron microscopy (SEM) analysis of cells in the L1 layer (epidermis on the

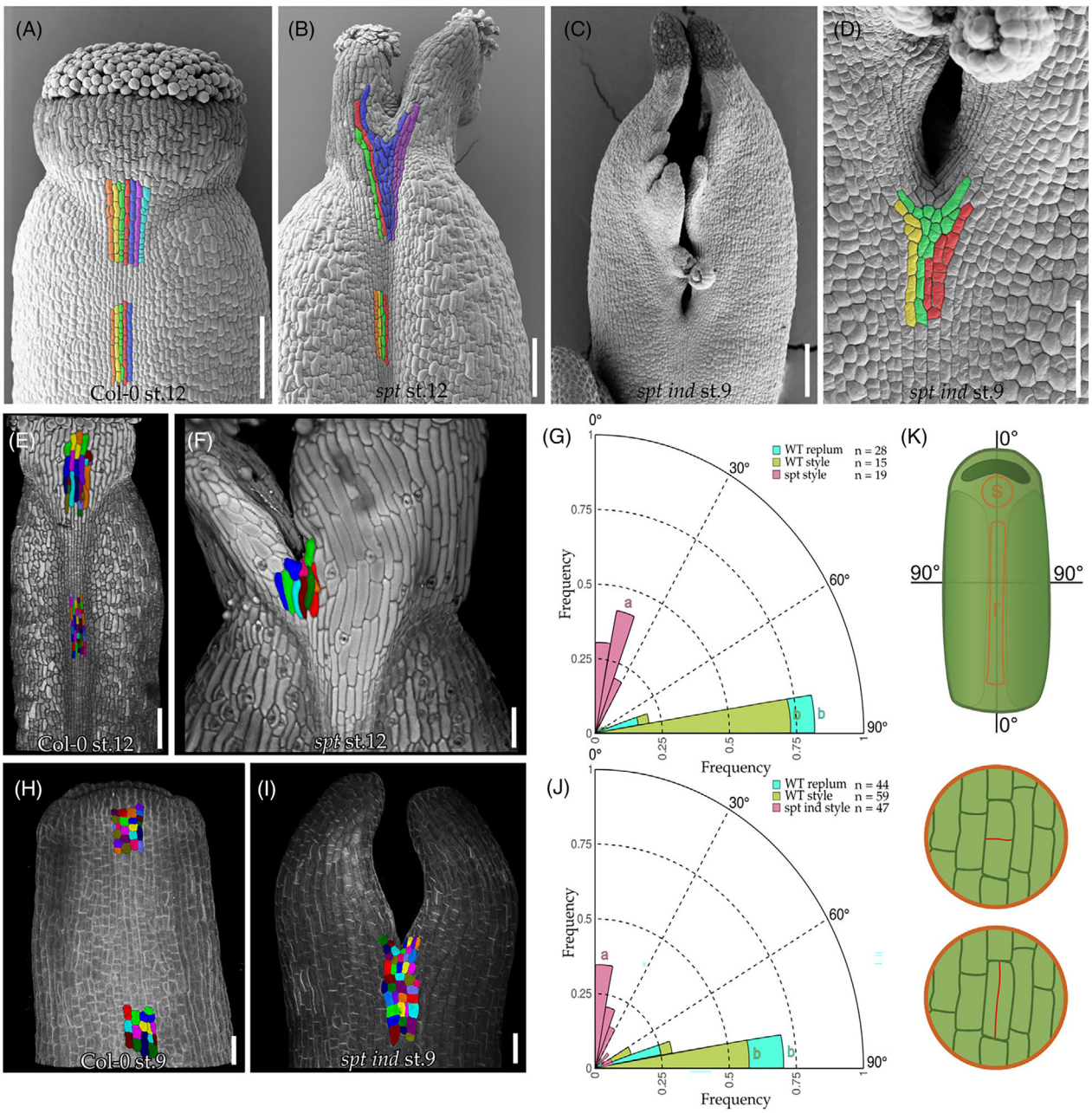

Figure 1. Deviation of the cell-division plane orientation at the onset of the *spt-12* and *spt-12 ind-2* split, bilateral style. (A–D) False-colored scanning electron micrographs (SEM) of (A, B) stage-12 (A) Col-0 and (B) *spt-12,* and (C, D) stage-9 *spt-12 ind-2* gynoecia, displaying cell files. (E, F) Confocal images of the L1 layer of stage-12 (E) Col-0 and (F) *spt-12* gynoecia stained with Calcofluor White and analyzed in MGX. (G) Quantification of the cell division angle from three biologically independent samples in Col-0 (WT) replum (n = 28) and style (n = 15) and *spt-12* style (n = 19) of stage-12 gynoecia. (H, I) Confocal images of the L1 layer of stage-9 (H) Col-0 and (I) *spt-12 ind-2* gynoecia stained with Calcofluor White and analyzed in MGX. (J) Quantification of the cell division angle from three biologically independent samples in Col-0 (WT) replum (n = 44) and style (n = 59) and *spt-12 ind-2* (n = 47) style of stage-9 gynoecia. Scale bars in (A–C) represent 100 μm, in (D) 50 μm, in (E) 100 μm, in (F) 50 μm, in (H) and (I) 20 μm. (K) Diagrammatic representation of the assessment of division plane orientation within Arabidopsis gynoecia. The figure depicts a stage 9 gynoecium, with the style and replum highlighted and labeled "s" and "r," respectively. The angles of division are illustrated with lines: a line parallel to the apical-basal axis represents 0°, while a line perpendicular to this axis, along the medial-lateral axis, represents 90°. Magnified insets (bottom) show cell divisions at these angles, with a red line indicating a 90° division in the top circle and a division at 0° in the bottom circle. The configuration of daughter cells post-division is deduced from the orientation of cell files and the thinner nature of the newly formed cell walls.

abaxial body-axis) of Col-0 (WT) style and replum tissues showed clear longitudinal alignment of cells along the apical-basal direction (Figure 1A), in agreement with strong anisotropic growth of these medial tissues (Eldridge et al., 2016; Gómez-Felipe et al., 2024). To quantify this alignment, we segmented high-resolution 3D confocal

microscopy image stacks of developing (stage 9) and mature (stage 12) WT gynoecia stained with Calcofluor White, which binds the cellulose present in the cell wall allowing visualization of the cellular outline (Herth & Schnepf, 1980), followed by segmentation via the image processing software MorphoGraphX (MGX) (Figure 1E,H; de Reuille et al., 2015; Strauss et al., 2022). Cell divisions were identified by analyzing cell geometry and wall properties, specifically occurring between cells of similar shapes featuring straight and thinner newly formed walls that initially lack pinching, highlighting early post-division changes (Figure 1K).

To define the cell division-plane orientation with respect to organ shape, a coordinate system was generated by placing a Bezier line to match the directions of the organ surface. This allowed us to define the specific division-plane orientation angle relative to the cells (Herth & Schnepf, 1980). These analyses show that the approximate division-plane orientation for stage-12 replum and style regions in Col-0 was 87.5° and 82.4°, respectively (Figure 1E,G). In the style of stage-9 WT gynoecia, the division-plane angle was 83.8° in the replum and 82.2° in the style (Figure 1H,J). Statistical analysis confirmed that the alignment of cells in the replum and style of developing and mature gynoecia was similar, in line with the observed anisotropic growth of these medial tissues (Eldridge et al., 2016; Gómez-Felipe et al., 2024).

While cells at the replum region of *spt-12* and *spt-12 ind-2* seemed still aligned in the apical-basal direction in a similar fashion to Col-0, we noticed that such alignment was compromised at the style region in both mutants, just at the onset of the apical cleft where the carpels are unfused (Figure 1B–D). In both mutants, cells did not align in longitudinal cell files and seemed randomly placed (Figure 1B–D). This suggests that to transit from bilateral symmetry in the ovary to radial symmetry at the style, cell-division orientation (and/or rate) might be orchestrated locally to form a continuous alignment of cells from the replum to the style (Figure 1A). To investigate the cellular basis orchestrating radial style development and understand how symmetry breaking can occur in mutant styles, we imaged the L1 layer of bilaterally symmetric mutant gynoecia apexes. To test whether deviation of cell-division orientation from the horizontal angle correlates with a break in radial symmetry at the style region, we compared stage-12 WT Col-0 and *spt-12* mutant gynoecia. The stylar region of mature *spt-12* styles exhibited an angle of approximately 15.3° (Figure 1F,G), displaying a misalignment in the orientation of division planes at the onset of the *spt-12* split style. This suggests that defects in cell-division orientation might be a causative factor of the split style phenotype. Considering the more severe bilateral style phenotype observed in the *spt-12 ind-2* double mutant compared to the *spt-12* single mutant (Figure 1C, D), a similar analysis was conducted on developing (stage 9) *spt-12 ind-2* styles. This aimed to quantify the cell-division orientation during the early phases of style development, particularly at the initiation of symmetry transition (Moubayidin & Østergaard, 2014). The analysis showed a statistically significant deviation of the average angle of approximately 17.5° at the apical, medial region of young *spt-12 ind-2* styles compared to WT (Figure 1I,J).

Altogether, our data confirm that deviation of cell division angle occurs at the onset of the medial-apical cleft in bilateral symmetric mutant styles.

Lack of auxin accumulation correlates with aberrant cell-division orientation at the medial-apical domain of spt mutant

Growth analysis studies of the WT gynoecium revealed that clones induced in the style expand along the apical-basal axis, creating single cell files that divide in the transverse anticlinal direction (Eldridge et al., 2016; Gómez-Felipe et al., 2024; Figure 1A). The transcription factor SPATULA governs style development by working from the medial tissues (Groszmann et al., 2008, 2010; Heisler et al., 2001), where it promotes a biradial state of auxin signaling distribution (Carabelli et al., 2021; Moubayidin & Østergaard, 2014). Auxin is known to influence cell geometry and control several aspects of organ patterning via regulating cell division and cell expansion (Yoshida et al., 2014). Moreover, a phospho-mimic mutant version of PIN1, fails to both accumulate auxin in the medial-apical cells and apically fuse the two carpels, similar to *spt* (Moubayidin & Østergaard, 2014). We therefore hypothesized that the morphogenetic signals promoted by auxin accumulation in the medial-apical cells would be required to maintain divisions oriented in the transverse anticlinal direction, similar to how division is oriented in the proximal medial tissue, the replum (Figure 1). If so, failure to accumulate auxin in the medial-apical cells would result in switching cell-division plane orientation and correlate with a break in radial symmetry.

To test whether deviation from the horizontal cell-division orientation observed in *spt* bilateral styles was due to lack of auxin accumulation at the medial-apical foci (Carabelli et al., 2021; Moubayidin & Østergaard, 2014), we crossed a fluorescent cell-division marker line, *35S::GFP:TUA6* (hereafter *TUA6:GFP*) (Ueda et al., 1998), which allowed visualization of the microtubule dynamics during mitosis, to an auxin signaling reporter (*DR5::RFP*) (Marin et al., 2010). This enabled the simultaneous determination of the earliest events of cell-division plane orientation in the auxin responsive cells, at the medial-apical region.

Confocal analysis of *TUA6:GFP;DR5::RFP* WT gynoecia at stage 9 of development, when the biradial (4-foci) stage of auxin accumulation is determined, showed a transverse anticlinal orientation of fundamental structures involved in

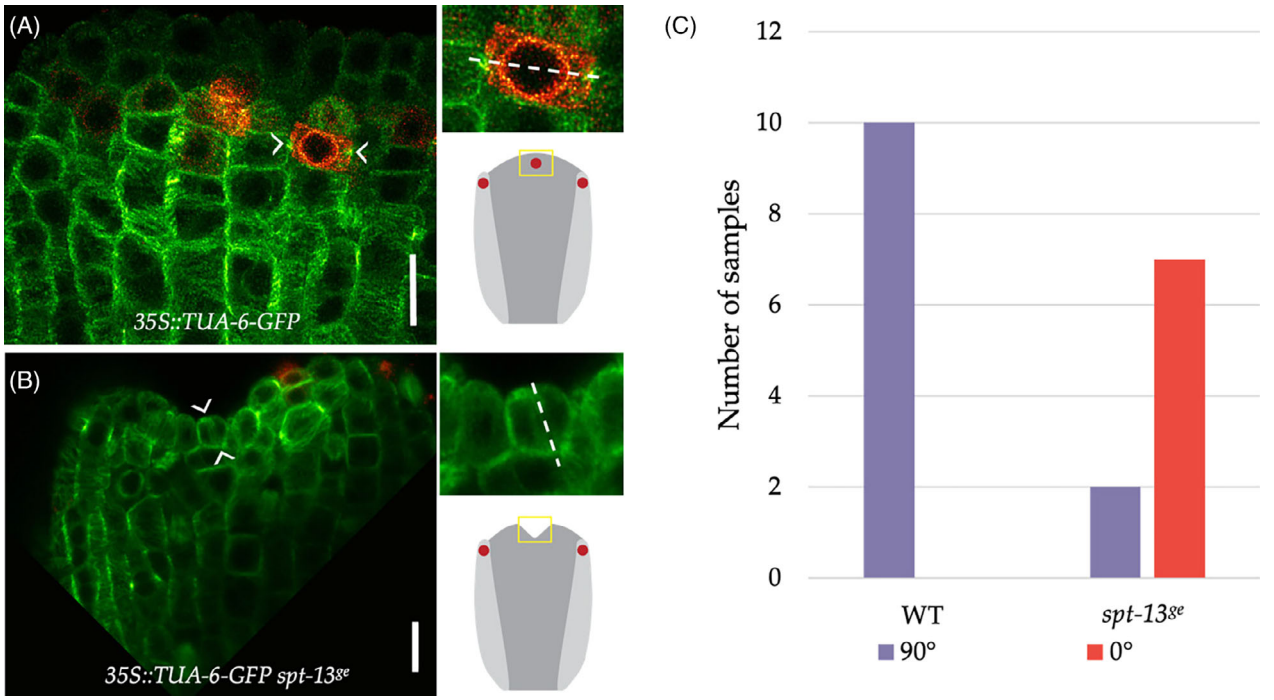

Figure 2. Lack of auxin accumulation in the medial-apical domain of *spt* bilateral style correlates with deviation of the cell-division angle. (A, B) Confocal image of stage-9 *TUA-6:GFP x DR5:RFP* gynoecium (inset, medial-apical domain) of (A) WT and (B) *spt-13*^{ge} backgrounds. The PPB (arrowheads) suggests the orientation of the future cell-division plate (dotted line) in dividing cells with or without auxin response (red cells/dots). Note, in (A), the auxin-responsive cell is dividing in the transverse anticlinal orientation; in (B), the PPB in the dividing cell where there has been no accumulation of auxin displays longitudinal anticlinal orientation. Scale bars represent 20 μm. (C) Number of samples collected for each genotype and type of division orientation observed in the medial domain of stage 8/9 gynoecia. 90° indicates transversal orientation (n = 10 in WT, n = 2 in *spt-13*^{ge}); 0° indicates longitudinal orientation (n = 0 in WT, n = 7 in *spt-13*^{ge}).

cell-division orientation, such as the pre-prophase band (PPB) (Figure 2A,C), correlating with anisotropic clones of auxin-responsive cells growing in the apical-basal direction (Figure S1).

In order to study whether cell-division orientation was altered owing to the absence of auxin accumulation in the medial-apical cells, a SPT mutant was produced using CRISPR/Cas9 (*spt-13*^{ge}) by transforming this construct in the *TUA6:GFP;DR5::RFP* background (Figure S2A,B). Homozygous *spt-13*^{ge}*;TUA6:GFP;DR5::RFP* gynoecia apexes displayed a break in radial symmetry (Figure S2B), correlating with absence of auxin signaling accumulation and misplacement of the PPB orientation (Figure 2B,C; Figure S1).

Altogether, these data corroborate the hypothesis that SPT controls cell-division orientation in the medial-apical auxin-responsive cells to keep the orientation of newly formed cell walls perpendicular to the direction of growth, which ultimately guarantees a continuum of cells in the medial tissues along the apical-basal direction, supporting anisotropic growth.

SPT promotes progression through cell-cycle G1-phase at the medial-apical gynoecium domain

SPT controls the dynamic distribution of auxin and the orientation of cell division (Figure 2). It is also known that SPT represses the cell-division input mediated by the hormone cytokinin (Reyes-Olalde et al., 2017; Figure 1B), a known auxin antagonistic signal (Moubayidin et al., 2009; Müller et al., 2017).

Thus, defects in the *spt* style might involve an altered cell cycle and/or growth rate. Recently, CYC-D3s, which promote progression through the G1-phase of the cell cycle, have been shown to coordinate cell proliferation and growth during changes in leaf shape (Li et al., 2024). In addition, *spt* hypersensitivity to CK applications (Reyes-Olalde et al., 2017) supports the hypothesis that failure to form a radially symmetric style might be due to ectopic proliferation, which in turn could accelerate the progression through the cell-cycle phases and alter the growth rate. Alternatively, a cleft at the medial domain could be caused by a delay or arrest in cell-cycle progression and overall growth.

To distinguish between these two scenarios, we analyzed a triple cell-cycle marker line (PlaCCI) (Desvoyes et al., 2020) in WT radial styles and mutant bilateral styles that allowed us to visualize nuclei in three consecutive stages of the cell-cycle: G1 (CFP-positive cells), S + early G2 (RFP- positive cells), and late G2 + M phases (YFP-positive cells). The ratio of G1/G2 cells was calculated to estimate the rate at which cells divide in *spt* mutant

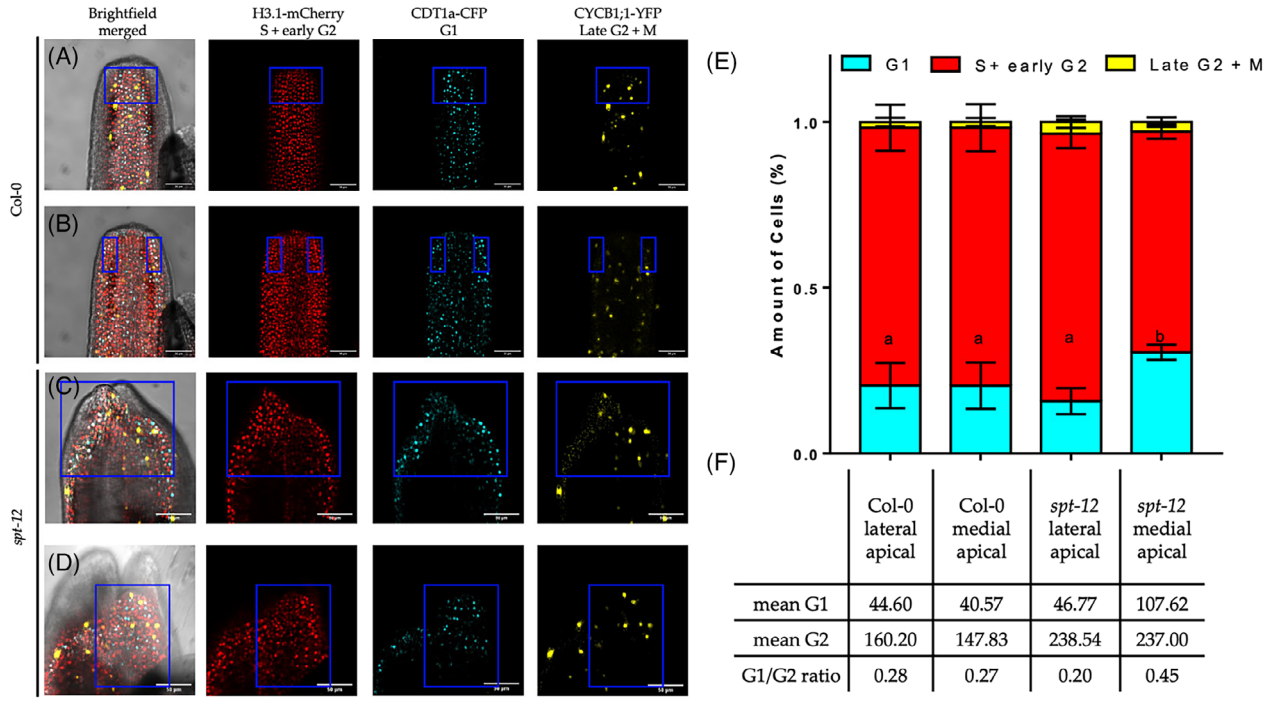

	Col-0 lateral apical	Col-0 medial apical	*spt-12* lateral apical	*spt-12* medial apical
mean G1	44.60	40.57	46.77	107.62
mean G2	160.20	147.83	238.54	237.00
G1/G2 ratio	0.28	0.27	0.20	0.45

Figure 3. The medial-apical region of the *spt* split-style displays slower progression of the cell-cycle G1-phase. (A–D) Confocal images of stage-9 gynoecia expressing PlaCCI reporter in (A, B) Col-0 and (C,D) *spt* (A, C) medial and (B, D) lateral domains. Scale bars represent 50 μm. (E) Quantification of proliferating cells in the gynoecia of Col-0 (n = 15 gynoecia) and *spt* (*n* = 13 gynoecia) in different cell cycle phases according to the signal of individual channels. The number of nuclei observed in each body domain and for each genotype is as follows: Col-0 lateral-apical (80 ~ 400); Col-0 medial-apical (80 ~ 350); *spt-12* lateral-apical (105 ~ 540); *spt-12* medial-apical (150 ~ 560). Error bars indicate standard deviation. Statistically significant different groups (lowercase letters) were determined by Fisher's exact test. (F) Table representing average number of nuclei in G1 and G2 cell-cycle phases in Col-0 and *spt* medial and lateral domains, and their respective ratio.

compared to wild type in the medial-apical region versus lateral-apical domain (Figure 3).

To understand whether patterning of the radial style depends upon coordinated proliferation along its circumference, which in turn would sustain coherent growth of its medial and lateral domains, we compared cell-cycle progression in the medial-apical region versus lateral-apical domain of the style in stage-9 gynoecia (Figure 3A,B). Our analysis showed that 20.5% of cells were in the G1 phase (average number of nuclei *n* = 40.5 in Col-0 medial-apical and *n* = 44.6 in Col-0 lateral-apical domains), while the remaining cells were collectively in the G2 phase (*n* = 147.8 in Col-0 medial-apical and *n* = 160.2 in Col-0 lateral-apical domains), with an overall ratio of G1/G2 nuclei 0.27 in both domains (Figure 3E,F). These data corroborate coordinated apical-basal anisotropic growth along the circumference of the style (Gómez-Felipe et al., 2024), *that is*, medial- and lateral-apical domains. Second, the analysis of the medial-apical domain of *spt* (Figure 3D) compared to WT showed a higher proportion of cells were in the G1 phase in the *spt-12* mutant: 30% of cells were in the G1 phase (*n* = 107.6; average number of G1 nuclei in the *spt-12* medial-apical domain) compared to the G2 phase (*n* = 237; average number of G2 nuclei in *the spt-12* medial-apical domain), with an overall ratio of G1/G2 nuclei 0.45 (Figure 3E,F). In contrast, the lateral-apical domain of *spt-12* (Figure 3C) did not show any statistically significant variation from the WT lateral and medial domain. It displayed that 15% of cells were in the G1 phase (*n* = 46.7 G1 and *n* = 238.5 G2 nuclei in *spt* lateral-apical domain), with an overall ratio of G1/G2 nuclei 0.19 (Figure 3E,F), half the ratio displayed from cells at the medial-apical domain of *spt*. These data suggest that the difference in cell-cycle progression is 2-fold lower at the *spt* medial- *versus* lateral-apical domains, supporting the hypothesis that SPT controls cell-division progression and presumably growth, specifically at the medial-apical domain.

Overall, our data has shown that nuclei at the inception of the bilateral cleft of *spt-12* are delayed in the G1 phase of the cell cycle, which suggests a slower cell cycle might be a contributing cause of the failure in radial symmetry establishment displayed by the *spt-12* mutant style. Also, these data argue against an augmented proliferation rate in the *spt-12* mutant that might be caused by de-repression of CK signaling and suggest that SPT promotes

G1-phase cell-cycle progression at the medial-apical region of the gynoecium apex undergoing the symmetry transition.

SPT and IND promote expression of CYC-D genes to support correct style morphogenesis

If SPT supports radial style development by promoting G1-phase progression (Figure 3), we would expect that core cell-cycle regulators promoting G1 and/or G1-S phase progression, such as cyclins, to be expressed at the style region and be positively regulated by SPT and its partner IND.

To test this, we analyzed available GUS transcriptional fusions of A-, B,- and D-type cyclins during gynoecium development (Figure S3).

D-type cyclin families (CYC-Ds) are canonically G1-phase promoting cyclins (Menges et al., 2006; Oakenfull et al., 2002). According to our hypothesis, three members of this family, CYC-D1;1, CYC-D3;2, and CYC-D3;3 are expressed at the gynoecium apex from early developmental stages, and then specifically expressed at the radial WT style (Figure 4A,B; Figure S3A). This is also in line with the role of CYC-D1;1 as a positive regulator of the G1 phase in embryos and ectopic cell divisions (Simonini et al., 2021), as well as the role of CYCD3s as regulators of proliferation and growth rate during leaf development (Li et al., 2024).

A-type cyclins (CYC-As) have been associated with the control of both mitosis and endoreduplication (Imai et al., 2006; Takahashi et al., 2010) and accordingly the transcriptional fusion of some members of this family, CYC-A2;3, CYC-A3;2, CYC-A3;3, and CYC-A3;4, were expressed specifically in the style as well as in the stigmatic tissue, where cells are elongated and hair-shaped (Figure S3B). Finally, B-type cyclins (CYC-Bs), which are considered true mitotic cyclins and promote the G2-M phase progression (Gutierrez, 2009), were not transcriptionally active at any developmental phase (Figure S3C), reflecting the quasi-meristematic nature of the carpels compared to primary meristems (Girin et al., 2009).

To understand whether G1-promoting cell-cycle regulators expressed in the style were positively regulated by SPT and IND, we analyzed CYC-D1;1 and CYC-D3;3 transcriptional GUS fusions in *spt* and *spt ind* backgrounds. We focused on these two specific regulators, as they have been shown to play key roles during the establishment and maintenance of the quiescent center cells of the root apical meristem (Forzani et al., 2014), which accumulate auxin (Sabatini et al., 1999). The expression of these two CYC-D members was strongly reduced *in vivo* at the bilateral *spt* style and barely detectable in the *spt ind* double mutant background (Figure 4A,B).

To corroborate a positive action of SPT and IND in promoting *CYC-Ds* expression, we performed *in vitro* qRT-PCR experiments. Firstly, to demonstrate that SPT is necessary to promote *CYC-D1;1* and *CYC-D3;3* expression, we analyzed *CYC-Ds* expression in loss-of-function *spt-12* inflorescences, which showed downregulation of both cyclin genes in the mutant background compared to WT levels (Figure S4A), resembling the *in vivo* results (Figure 4A,B). To demonstrate that SPT is also sufficient to control *CYC-Ds* expression, we used a *SPT* overexpressing transgenic line (*35S::SPT-FLAG*) with increased levels of *SPT* in both inflorescences and seedlings (Figure S4B,C) and demonstrated that up-regulation of SPT from seedlings is sufficient to increase the expression levels of both cyclin genes (Figure 4C). Notably, radialization of the first true leaves by IND overexpression requires SPT function (Moubayidin & Østergaard, 2014), demonstrating that both transcription factors are required for altering organ shape and that their activity in leaves can be assessed for sufficiency of their functions.

To further corroborate a role for IND in this process, we performed qRT-PCR experiments using an inducible overexpressing line of IND, *35S::IND-GR* (Sorefan et al., 2009), which is sufficient to impose radial symmetry in gynoecia and leaves (Moubayidin & Østergaard, 2014; Sorefan et al., 2009). We analyzed the transcription levels obtained from 7-day-old seedlings treated for 24 h with Dexamethasone (DEX) to induce overexpression of IND, which led to upregulation of both *CYC-D1;1* and *CYC-D3;3* expression compared to mock-treated seedlings (Figure 4D), altogether demonstrating that also IND is necessary and sufficient to upregulate these G1-promoting cyclins.

Finally, to support a role for a SPT/IND-mediated control of D-type cyclins in style development, we looked at the loss-of-function *cyc-d1;1* single mutant as well as *cyc-d1;1 cyc-d3;3* double mutant (Forzani et al., 2014). None of the genotypes observed showed defects in style formation (Figure 5A,C,E), *that is*, mis-regulation of the G1 phase is not sufficient *per se* to break style radial symmetry, supporting a scenario where multiple pathways are mis-regulated in the bilateral style of *spt* and *spt ind*.

Since the *spt* phenotype is exacerbated by the mutation in *ind* (Figure 5H; Girin et al., 2011) and IND also upregulates *CYC-Ds* expression (Figure 4D), we predicted that removing CYC-Ds function in a *spt* background should produce a more severe split-style, like *spt ind*. While *spt cyc-d1;1* were indistinguishable from the segregating *spt* control (Figure 5B,F), both *spt cyc-d3;3* double and *spt cyc-d1;1 cyc-d3;3* triple mutant split-styles were increasingly more affected (Figure 5D,G). These data show a novel, specific role for core cell-cycle regulators in controlling style formation, specifically symmetry transition at the gynoecium apex. Altogether, our data shows that SPT promotes progression through the G1 phase of the cell cycle at the medial-apical domain (Figure 3), by promoting, alongside IND, the expression of specific *CYC-Ds*, core regulators of

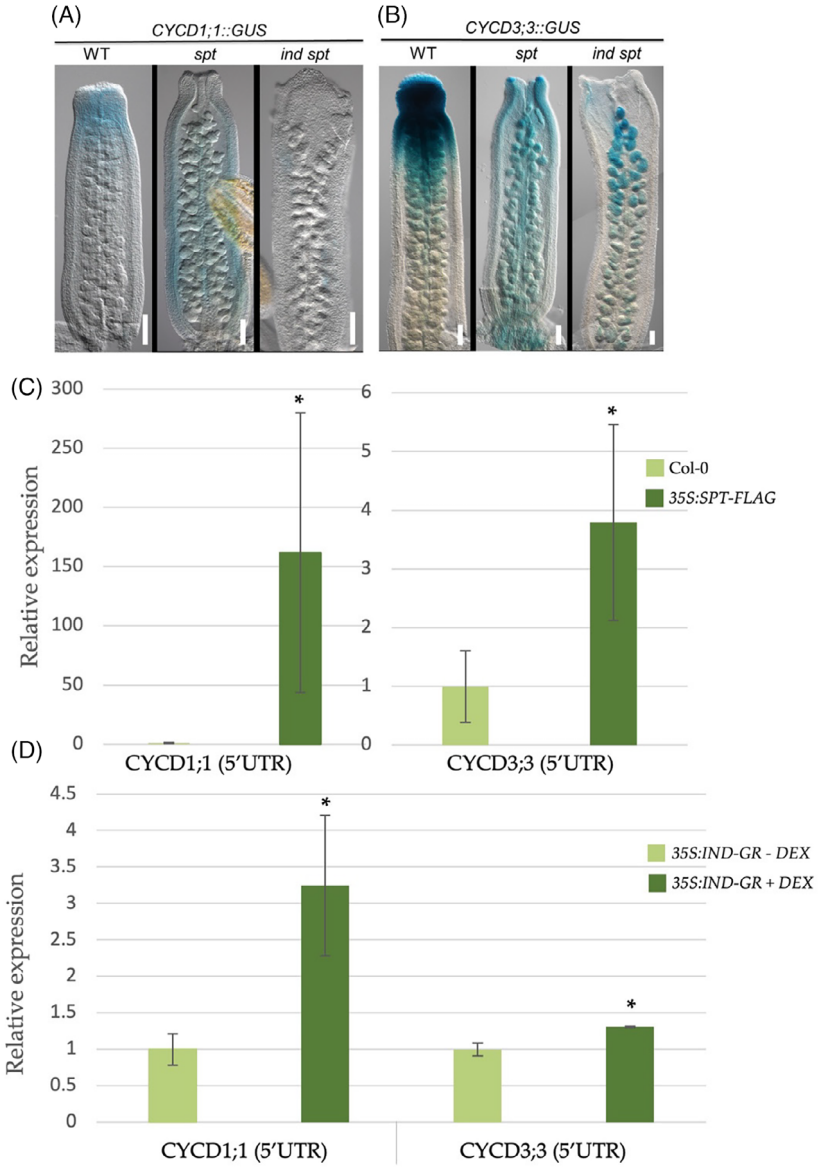

Figure 4. SPT and IND promote the expression of *CYC-D1;1* and *CYC-D3;3* genes. (A, B) Optical micrographs showing the *in vivo* expression of (A) *CYC-D1;1*::*GUS* and (B) *CYC-D3;3*::*GUS* in WT (left panel), *spt-12* (middle panel), and *spt-12 ind-2* (right panel) stage-12 gynoecia. Scale bars represent 100 μm. (C) qRT-PCR experiments showing significant increase in the expression levels of (left) *CYC-D1;1* and (right) *CYC-D3;3* in *35S*::*SPT-FLAG* seedlings (dark green columns) compared to Col-0 (light green columns). Bars indicate mean ± SE (n = 3). Statistically significant different groups (asterisks) were determined by Turkey's test (*$P < 0.05$). (D) qRT-PCR experiments showing significant increase in the expression levels of (left) *CYC-D1;1* and (right) *CYC-D3;3* after 24 h Dex treatment (dark green columns) compared to mock (light green columns) of *35S*::*IND-GR* seedlings. Bars indicate mean ± SD ($n = 3$), and asterisks indicate significant differences by Student's *t*-test (*$P < 0.05$).

the cell cycle, whose function is important for correct style development.

SPT and IND orchestrate an incoherent type-I feed-forward regulatory loop converging on CYC-Ds

Our data suggest a coupling exists to coordinate cell division and auxin accumulation for the establishment of a radially symmetric style (Figure 2). The transcriptional regulatory regions of *CYC-D1;1* and *CYC-D3;3* loci, such as promoter, 5′- and 3′-Untranslated Regions (UTRs), have multiple *cis*-elements recognized by bHLH transcription factors (Toledo-Ortiz et al., 2003; Figure 6A,D). SPT recognizes the canonical bHLH transcription factor *cis*-element G-box sequence (*CACGTG*), while IND preferentially binds the E-variant (*CACGCG*) sequence (Girin et al., 2010), which suggests that the regulation of *CYC-Ds* by SPT and IND might be direct. In addition, several AuxRE-box (Auxin Response Element, *TGTCTC*) (Boer et al., 2014;

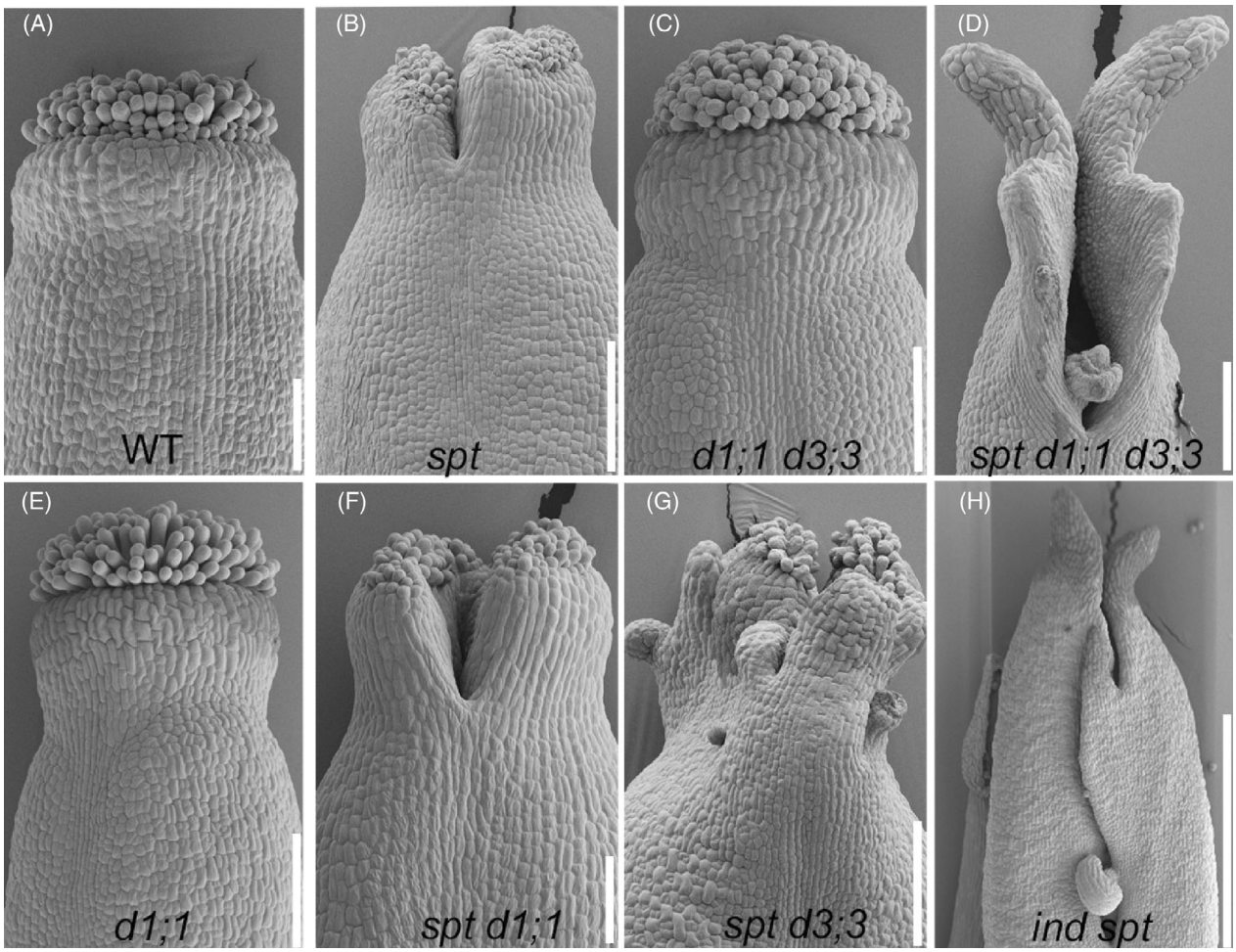

Figure 5. The activity of CYC-D1;1 and CYC-D3;3 promote radial style morphogenesis. (A-H) SEM phenotypes of stage-12 (A) Col-0 WT, (B) *spt-12* (C) c*yc-d1;1 cyc-d3;3*, (D) *spt-12* c*yc-d1;1 cyc-d3;3*, (E) c*yc-d1;1*, (F) *spt-12 cyc-d1;1*, (G) *spt-12 cyc-d3;3* and (H) *ind-2 spt-12* gynoecia. Scale bars represent 100 μm.

Guilfoyle, 2015), which is typically recognized by the Auxin Response Regulators (ARFs), which start transcription in response to auxin, were also present on both *CYC-Ds* regulatory regions (Figure 6A,D). IND has been tightly linked to auxin signaling by, among others, its direct protein–protein interaction with ARF3/ETTIN (hereafter, ETT) transcription factor (Simonini et al., 2016). ETT works as an uncanonical auxin receptor, and the IND-ETT interaction is disrupted by auxin, that is, auxin-sensitive (Kuhn et al., 2020; Simonini et al., 2016). Interestingly, in the 3′UTR of CYC-D1;1 we noticed a 1 bp-overlap between a G-box element and an AuxRE-box (Figure 6A). This raised the interesting hypothesis that the molecular interaction among gynoecium regulators and auxin might be antagonistic and/or competitive.

To test this hypothesis, we initially conducted Chromatin Immunoprecipitation (ChIP) experiments using 7-day-old seedlings of *35S::IND:GR* line (Sorefan et al., 2009) and 24 h of DEX induction. We found that IND could bind both 5′ and 3′ UTRs of *CYC-D1;1* after DEX treatment (Figure 6C) and a region in the promoter of *CYCD3;3* (Figure 6E). Interestingly, 3 h of auxin application, whose *in vivo* distribution is controlled by IND (and SPT) (Girin et al., 2010; Ichihashi et al., 2010; Moubayidin & Østergaard, 2014), impaired IND from binding *CYC-D1;1* and *CYCD3;3* regulatory regions (Figure 6C,E). These results show that on one hand, IND (and presumably SPT) bind directly to *CYC-D1;1* and *CYC-D3;3* while, on the other hand, auxin plays a negative effect on the IND-mediated binding of *CYC-Ds*. Since IND promotes both *CYC-Ds* expression and auxin accumulation, this suggests an incoherent feed-forward regulatory loop converging on *CYC-D1;1* and *CYC-D3;3* expression.

To test this molecular regulation, we performed qRT-PCR experiments using *35S::IND-GR* seedlings were treated with mock and DEX in the presence or absence of 50 μM Indole-3-Acetic Acid (IAA) in the growing medium for 3 h. The *in vitro* analysis showed that auxin works in an

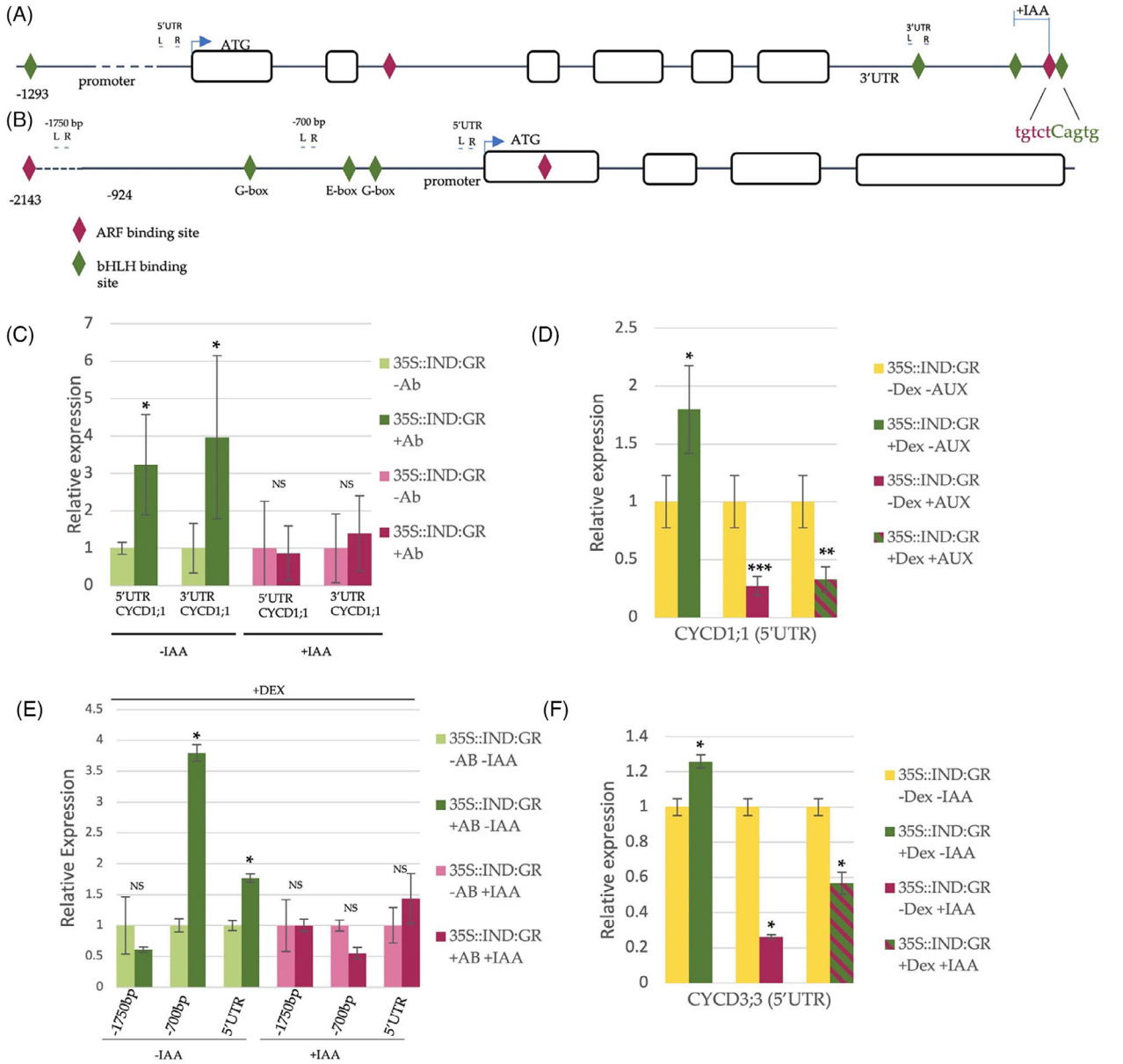

Figure 6. Molecular control of *CYC-D1;1* by IND and auxin reveals an incoherent feed-forward regulatory loop. (A, B) Diagram of the (A) *CYC-D1;1* and (B) *CYC-D3;3* loci displaying their promoter, 5′UTR, exons, introns, and 3′UTR. The location of the ARF binding sites (purple diamonds), the bHLH binding sites (G-box and E-box, green diamonds), and primers used in this study are shown. Note, a 1 bp-overlap between a G-box (*CACGTG*) and an AUX-RE box (*TGTCTC*) at the *3′UTR* of *CYC-D1;1*. (C) ChIP q-PCR experiments using *35S::IND-GR* seedlings induced by Dexamethasone (Dex) showing IND direct binding to the *CYC-D1;1* locus (*5′UTR* and *3′UTR*) (green columns) only in the absence of Auxin (-IAA). Following IAA applications, (+IAA, purple columns) IND binding to *CYC-D1;1 5′UTR* and *3′UTR* regions is lost. Bars indicate mean ± SD ($n = 3$), and asterisks indicate significant differences by Student's *t*-test (*$P < 0.05$; n.s. not significant). (D) qRT-PCR of *35S::IND-GR* seedlings induced by Dex and/or IAA compared to mock (yellow columns) showing the relative expression of *CYC-D1;1* after IND upregulation (green columns), auxin application (purple columns), and both (green/purple columns). Bars indicate mean ± SD ($n = 3$), and asterisks indicate significant differences by Student's *t*-test (*$P < 0.05$; **$P < 0.01$; ***$P < 0.001$). (E) ChIP q-PCR experiments of *35S::IND-GR* seedlings induced by Dex showing IND direct binding to the *CYC-D3;3* locus (primers −700 bp and 5′UTR, green columns) only in the absence of Auxin (−IAA). Following IAA applications, (+IAA, purple columns) IND binding to *CYC-D3;3* promoter regions were lost. Bars indicate mean ± SD ($n = 3$), and asterisks indicate significant differences by Student's *t*-test (*$P < 0.05$; n.s. not significant). (F) qRT-PCR of *35S::IND-GR* seedlings induced by Dex and/or IAA compared to mock (yellow columns) showing the relative expression of *CYC-D3;3* after IND upregulation (green columns), auxin application (purple columns), and both (green/purple columns). Bars indicate mean ± SD ($n = 3$), and asterisks indicate significant differences by Student's *t*-test (*$P < 0.05$).

antagonistic and epistatic manner to IND in regulating *CYC-D1;1* and *CYC-D3;3* expression: while IND induces *CYC-Ds* expression, auxin represses it (Figure 6D,F). Moreover, when auxin and DEX were both present, the overexpression of *CYC-D1;1* and *CYC-D3;3* expression caused by IND was strongly inhibited or absent (Figure 6D,F).

Altogether, these data show fine-tuned control on cell-cycle regulation operated by IND and SPT: IND and SPT promote the expression of *CYC-D1;1* and *CYC-D3;3* and control the accumulation of auxin, which in turn shuts down *CYC-Ds* expression. This type of transcriptional regulation resembles an Incoherent-type-I feed forward loop, which in biology has been shown to generate pulses of gene expression and provide an efficient way for cells to detect fold-changes in gene products (Alon, 2007; Goentoro et al., 2009). As the expression of cell-cycle regulators is pivotal in morphogenesis, an Incoherent-type-I Feed Forward Loop is consistent with tight regulation of CYC-Ds protein levels in cells with different auxin levels. The incoherent feed-forward regulatory loop orchestrated by SPT and IND might presumably coordinate proliferation and growth rate via fine-tuning G1-phase progression, with orientation of the cell-division angle in a spatio-temporal manner (Figure 7).

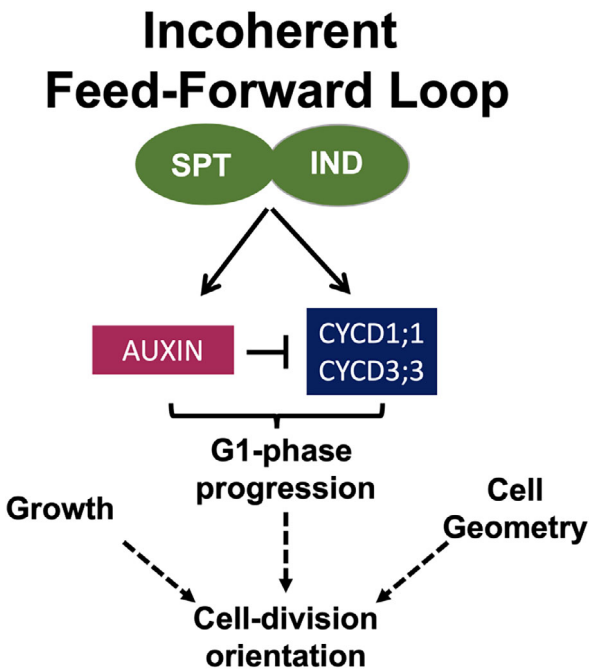

Figure 7. An Incoherent Feed-Forward regulatory loop controls G1-phase progression and style morphology. Speculative model for the control of cell division during style radialization at the gynoecium apex. Two bHLH transcription factors, SPT and IND, promote the expression of G1-phase regulators, *CYC-D1;1* and *CYC-D3;3*, in an opposite manner to auxin, whose accumulation depends on SPT and IND (Moubayidin & Østergaard, 2014). This creates an Incoherent type-I Feed-Forward regulatory loop that fine-tunes *CYC-Ds* expression and the G1-phase progression, presumably by turning on and off their expression in a cell-specific manner according to the hormonal concentration. Ultimately, this mechanism can add robustness to the placement of the cell-division angle, which can also be affected by growth dynamics and topological aspects, *for example*, cell geometry.

DISCUSSION

During development of the Arabidopsis female reproductive organ, a symmetry transition event—from bilateral symmetry in the ovary to radial symmetry at the apical style—has been shown to require dynamic distribution of auxin to form a ring of hormone maximum at the apex of the gynoecium (Moubayidin & Østergaard, 2014). Auxin has been shown to be important to regulate cell division plane orientation in multiple contexts (Chakrabortty et al., 2018; Cruz-Ramírez et al., 2012; De Rybel et al., 2013; Yoshida et al., 2014). In the gynoecium, the regulation of auxin dynamics is under the control of various transcription factors, including SPT, IND, and HECATEs (Groszmann et al., 2011; Moubayidin & Østergaard, 2014), but the effect that the auxin ring plays on local cellular dynamics is still unclear. Notably, the lack of auxin maxima in the medial foci in the *spt* mutant (Figure 2; Moubayidin & Østergaard, 2014) allowed the effect of the auxin maxima on cellular dynamics to be inferred, specifically during style formation. Thus, comparing the *spt* and *spt ind* mutants to Col-0 is an excellent system to understand the cellular, genetic, and molecular bases of radial style formation and elucidate how the apical fusion of the carpels occurs.

This work has explored the hypothesis that cell-division plane orientation and progression through the G1-phase of the cell cycle are coordinated with the auxin dynamics during the symmetry transition at the gynoecium apex. Our data provides the cellular basis for how a break in radial symmetry occurs in mutants of key regulators of Arabidopsis style development, SPT and IND (Figure 7). Via quantitative confocal analysis, we pinpointed defects in cell-division orientation in bilaterally symmetric *spt* and *spt ind* styles (Figure 1F,I). We linked defects in cell-division orientation observed in *spt* specifically to the lack of auxin accumulation in the medial-apical cells (Figure 2), which is promoted and built-up by the activity of SPT and IND (Moubayidin & Østergaard, 2014). Analyzing a triple cell-cycle marker proved that divisions in the *spt* bilateral style are delayed in the G1-phase of the cell-cycle (Figure 3), correlating with a much-reduced expression of *CYC-D1;1* and *CYC-D3;3* at the apical style (Figure 4). We established that both CYC-D1;1 and CYC-D3;3 are genetically and molecularly downstream targets of SPT and IND (Figures 4, 5, and 6). Ultimately, our data showed a negative regulation of *CYC-Ds* expression is triggered by auxin and correlates with the inhibition through (at least) IND direct binding to the regulatory regions of *CYC-D1;1* and *CYC-D3;3* in the presence of auxin (Figure 6).

One possible scenario that fits our data is consistent with a temporal, stage-specific regulation of *CYC-Ds* by SPT and IND, which likely influences CYC-Ds protein expression through auxin cellular levels. In this scenario, at early stages of style development, SPT and IND promote the expression of the G1-phase-promoting cell-cycle regulators, while as auxin peaks, *CYC-Ds* transcriptional regulation is switched off, resulting in an incoherent type-I

feed-forward loop mechanism (Mangan & Alon, 2003). This mechanism could generate a pulse of CYC-Ds protein expression according to the auxin cellular levels and thus coordinate the rate of cell division and growth with the orientation of the cell-division angle (Figure 7), which ultimately would support anisotropic growth in the style region (Eldridge et al., 2016; Gómez-Felipe et al., 2024). Likely, more than one distinct cell division activity underpins this morphological process, and their coordination must be tightly regulated in space and time by master regulators, such as SPT and IND. It is not understood how SPT and IND interact with auxin to regulate *CYC-Ds* expression and whether this regulation is based on the known auxin-sensitive interaction between IND and the auxin response factor ETT/ARF3 or employs the TIR/AFBs-mediated canonical auxin pathway (Simonini et al., 2016).

Thus, we propose a working model (Figure 7) that underpins the cellular basis of radial style morphogenesis: two bHLH transcription factors (IND and SPT) and auxin fine-tune the expression of *CYC-Ds* to coordinate the progression through the G1-phase of the cell cycle. We speculate that this mechanism might add robustness to the placement of the cell-division plane in the auxin-responsive cells, allowing carpel fusion at the medial-apical domain. Altogether, this mechanism would coordinate cell division rate and orientation, necessary to support correct anisotropic growth in the style region (Figure 7). Although, whether the switch in cell division orientation is a cause of the bilateral style or a consequence of changes in growth pattern of neighboring tissues and/or cellular topologies, *for example*, cell geometry, is also possible, it is still an open question (Figure 7).

To understand the causative mechanisms of cell division misorientation at the gynoecium apex would require careful employment of genetic tools and live/time-lapse imaging to discern the effects of mechanical stresses during growth from its genetics components.

How plants orient the division plane remains an area of intense research because there are many factors that influence this process (Hartman & Muroyama, 2023; Rasmussen & Bellinger, 2018), and it is a fundamental strategy that plants adopt to promote patterning (Chakrabortty et al., 2018). Auxin does promote cell cycle progression, which has been linked to cell division orientation (Costa, 2017; Yoshida et al., 2014). Whether the misorientation of the cell division plane causes the *spt-12* phenotype or is a consequence of changes in the growth pattern of tissues is still an open question. During style development, SPT is an important medial-lateral regulator and, moreover, positively promotes the expression of adaxial regulators (Carabelli et al., 2021). It is thus possible to speculate that in the *spt* mutant background, uncontrolled direction and/or rate of growth across tissues and body domains might re-orient cell division in the epidermal cells.

Striking evidence has shown that early cues, occurring in the G1 phase of the cell cycle, feed into the determination of the division plane in plants: accelerating the G1/S transition, either genetically via CYC-D function or pharmacologically, can enhance division plane defects in root tissues (Costa, 2017). This suggests either a division plane-orienting cue acts in G1 phase or slowing down the rate of proliferation is required to facilitate proper division orientation. In addition, our findings are also in line with a recent investigation unveiling that CYC-D3s play pivotal roles in orchestrating timing and morphology from cells to organs in the shape acquisition of Arabidopsis juvenal versus mature leaves by coordinating cell proliferation and growth (Li et al., 2024).

Overall, whether cell-division orientation at the gynoecium apex contributes to the formation of a fused style (via the genetic control mediated by SPT and IND on the G1-phase regulators, CYC-Ds) or is an indirect consequence of miss-regulated growth, remains to be elucidated, that is, changes in cell-division orientation observed at the onset of the split-style could be a consequence of changes in directional growth and tissue mechanical stresses rather than its cause.

Nevertheless, the activity of the master regulators SPT and IND and their downstream targets CYC-D1;1 and CYC-D3;3 during radial style development is somehow reminiscent of that reported for WOX5 (WUSCHEL RELATED HOMEOBOX 5) during the establishment and maintenance of the root apical stem cell niche (Forzani et al., 2014). At the root tip, the master regulator WOX5 represses CYC-D1;1 and CYC-D3;3 expression in the quiescent center, where cells do not (usually) divide and accumulate high auxin (Forzani et al., 2014). The up-regulation of both *CYC-Ds* is causative of the ectopic cell divisions displayed by the QC cells of the *wox5* single mutant and, therefore, correct patterning of the root stem cell niche can be restored by removing CYC-D1;1 and CYC-D3;3 functions from the *wox5* background (Forzani et al., 2014). Interestingly, in both roots and gynoecia, the activity of CYC-D3;3 seems to have stronger effects compared to CYC-D1;1 alone, as the double *wox5 cyc-d3;3* (Forzani et al., 2014) and *spt cyc-d3;3* (Figure 5) mutants have an effect on the phenotypes observed, while *wox5 cyc-d1;1* (Forzani et al., 2014) and *spt cyc-d1;1* (Figure 5G) do not, unless in combination in a triple mutant with the above partners, in a synergistic fashion. Even though we still do not understand the genetic and mechanistic reasons to explain the nuances of these phenotypes, it suggests that a conserved mechanism could be in place at the tips of roots and gynoecia, where auxin maxima peak, to regulate cell division via the activity of organ-specific master regulators and their downstream control on *CYC-D1;1* and *CYC-D3;3* expression. The key difference between the two developmental contexts is that while at the root tip, cell division is suppressed in the

auxin-maxima QC cells via WOX5 (Forzani et al., 2014), at the gynoecium apex, cell division is promoted via SPT and IND (this work).

Our data from the L1 epidermis fits well with the strong anisotropic growth requirements discovered for the abaxial style cells (Eldridge et al., 2016; Gómez-Felipe et al., 2024). Furthermore, a recent investigation of the *O*-Glycosyl transferases SECRET AGENT and SPINDLY, upstream regulators of SPT function during style morphogenesis, revealed fundamental roles for these enzymes in style cellular elongation (Jiang et al., 2024), which is also in line with the strong anisotropic growth displayed by the abaxial epidermal cells (L1) of the style (Eldridge et al., 2016; Gómez-Felipe et al., 2024).

Our cellular analysis performed in the L1 layer suggests that SPT and IND coordinate cell-division rate and/or orientation with auxin accumulation. A tissue-level model (simulating the L1 layer, abaxial epidermis) showed that a specific growth rate oriented by a proximodistal polarity field is sufficient to simulate the formation of a fused (radial) style (Eldridge et al., 2016). In addition, genetic studies demonstrated that the *spt* split-style phenotype could be partially rescued by elimination of the activity of the boundary genes CUP SHAPED COTYLEDON 1 (CUC1) and CUC2: analysis of the *spt cuc1 cuc2* triple mutant revealed that a fused style can form from the abaxial tissues (epidermis) and can be hollowed from the inside, that is, no adaxial vascular tissues developed within the style (Nahar et al., 2012).

These two studies strongly highlight that growth along these two domains (adaxial and abaxial) can be uncoupled during style morphogenesis and must be coordinated to contribute to the optimum shape of the style.

Several key molecular players involved in controlling cell-division orientation and proliferation have been characterized in Arabidopsis and linked to specific plant development processes, often via genetic interaction with hormonal transduction pathways (Chakrabortty et al., 2018; Cruz-Ramírez et al., 2012; De Rybel et al., 2013; Yoshida et al., 2014). While many studies have elucidated the contribution of auxin (and other phytohormones) in orchestrating either cell-division orientation or rate of proliferation in development, very little is known about how these two cell-division activities, occurring at different phases of the cell cycle, are coordinated to one another during plant organogenesis.

A well-studied example of the complexity of the interaction between the cell cycle, auxin, and transcription factor activity involves CYC-D6;1 and its function in patterning tissues within the root. Two successive asymmetric cell divisions (ACDs) in the Arabidopsis root meristem generate endodermis and cortical tissues. SHORT ROOT (SHR) and SCARECROW (SCR) transcription factors, members of the GRAS family, are important heterodimers for ACD and play a prominent role in the maintenance and specification of the root stem cell niche (SCN), where an auxin maximum peaks (Cruz-Ramírez et al., 2012; Moubayidin et al., 2016). CYC-D6;1 is a direct transcriptional target of SCR and its partner SHR (Sozzani et al., 2010), which resembles our proposed direct and positive activity of SPT and IND in controlling *CYC-D1;1* and *CYC-D3;3* expression at the gynoecium apex. Control of *CYC-D6;1* expression by SCR and SHR is reduced by a stem cell-associated auxin maximum (Cruz-Ramírez et al., 2012) to prevent further formative divisions. Interestingly, a recent investigation showed that SHR and SCR act specifically at the G1-phase of the cell cycle to promote formative, asymmetric cell division via upregulation of *CYCD-6;1*, while their later expression in G2 and M phases does not exert the same effect, leading to a switch to proliferative, symmetric division (Winter et al., 2024). Via this elegant mechanism, the dimer SCR/SHR coordinate organ patterning (via asymmetric, formative divisions) and growth (via symmetric, proliferative divisions) (Winter et al., 2024). It would be interesting to assess whether SPT and IND also act in a specific phase of the cell cycle to regulate *CYC-Ds* expression and whether any switch from symmetric to asymmetric cell division occurs in the auxin responsive cells undergoing symmetry transition and its link to style fate determination.

During early phases of embryogenesis, auxin accumulation is essential for protodermal patterning as it allows to override a default division that would otherwise occur along the shortest wall path. This auxin-mediated control of cell-division orientation generates an asymmetric separation of the initial cell in two unequal daughter cells, thus driving the first separation between the inner and outer tissues that gives rise to the epidermal cell layer (Yoshida et al., 2014). Division of the auxin-responsive cells at the medial-apical region of the gynoecium is *in bona* symmetric. In this context, it is possible to speculate that maybe the accumulation of auxin might be required to maintain anticlinal orientation of division—parallel to the divisions occurring within the replum tissue below the style—to merge the unfused top of the two carpels.

Another fascinating case that links duration of G1-phase and auxin dynamics to an asymmetric-to-symmetric cell-division switch occurs during the stomata lineage. Although, in this developmental context, it is the depletion of auxin to be required to make the switch from asymmetric to symmetric division, which forms the guard mother cell (Le et al., 2014). In addition, the length of the G1-phase is faster in asymmetrically dividing (proliferating) cells compared to those committed to divide symmetrically (to differentiate), thanks to the activity of a specific bHLH transcription factor, MUTE, and its downstream positive regulation of a cell-cycle inhibitor SIAMESE-RELATED4 (SMR4) (Han et al., 2022). SMR4 works as a break for the cell cycle by slowing down the G1-phase via its direct interaction

with CYC-D3;1, a positive regulator of proliferative asymmetric divisions in the meristemoid cells (Han et al., 2022; MacAlister et al., 2007). Therefore, the interplay between auxin dynamics, G1-phase duration, and bHLH transcription factors connects patterning and growth in the stomata lineage as well as at the style.

SPT promotes differentiation of the apical style by sustaining auxin distribution, while it also represses the cell-division input promoted by the hormone cytokinin (Zhang et al., 2016). This is consistent with the known SPT function as a negative regulator of organ growth (in leaves and roots) (Ichihashi et al., 2010; Makkena & Lamb, 2013) and the antagonistic activity of auxin and cytokinin during plant organ patterning, including gynoecium development. The activity of this master regulator is tightly controlled in time and space. Thus, it is possible to speculate that SPT and IND might directly control a plethora of cell-cycle regulators in a tissue- and temporal-specific manner, but the output of their transcriptional regulation might be influenced by local concentrations of hormones, that is, auxin and cytokinin. In this scenario, other regulatory transcriptional loops, in addition to the incoherent feed-forward loop unveiled in this study, might explain why SPT and IND act as positive or negative regulators of organ growth in different developmental contexts or temporal windows.

In conclusion, this work has unveiled the cellular basis that underpins radial style shape acquisition of the Arabidopsis gynoecium, and it provides a platform to investigate how coordination of cell division and growth can impact the morphology of the female reproductive organ.

MATERIALS AND METHODS

Plant materials and growth conditions

Seeds were surface sterilized in a solution of 50% ethanol and 4 mg/ml of dichloroisocyanurate for 10 min, and subsequently washed with sterile water three times. The seeds were stratified in a 0.1% sterile agarose solution at 4°C in the dark for 5 days, before being sown on MS media plates containing 0.8% agar and 1% sucrose. Seedlings were grown vertically for 7 days (unless specified) under long-day conditions (16 h light/8 h dark) at 22°C and 70% humidity. Seedlings were then transferred to soil and grown in a controlled environment room under long-day conditions (16 h light/8 h dark; 22°C) and 70% humidity.

Mutant lines *spt-12* (Ichihashi et al., 2010), *spt-12 ind-2* (Girin et al., 2011) *35S::IND:GR* (Sorefan et al., 2009), *TUA6-GFP* (Ueda et al., 1998), *DR5:RFP* (Marhavý et al., 2011), PlaCCI triple cell-cycle marker (Desvoyes et al., 2020), *cyc-d1;1* (Forzani et al., 2014), *cyc-d1;1 cyc-d3;3* (Forzani et al., 2014), CYC-D1;1::GUS, *CYC-D3;1::GUS*, *CYC-D3;2::GUS*, *CYC-D3;3::GUS*, *CYC-D4;2::GUS*, *CYC-D5;1::GUS*, *CYC-D6;1::GUS*, *CYC-D7;1::GUS* (Collins et al., 2012); *CYCA1;1::GUS* (N799889), *CYCA2;2::GUS* (N799890); *CYCA2;3::GUS* (N799891) (Bulankova et al., 2013), *CYCA2;4::GUS* (N799892) (Bulankova et al., 2013), *CYCA3;1::GUS* (N799893) (Bulankova et al., 2013), *CYCA3;2::GUS* (N799894) (Bulankova et al., 2013), *CYCA3;3::GUS* (N799895) (Bulankova et al., 2013), *CYCA3;4::GUS* (N799896) (Bulankova et al., 2013), *CYCB1;2::GUS* (N799897) (Bulankova et al., 2013), *CYCB1;4::GUS* (N799898) (Bulankova et al., 2013), *CYCB2;1::GUS* (N799899) (Bulankova et al., 2013), *CYCB2;2::GUS* (N799900) (Bulankova et al., 2013), *CYCB2;3::GUS* (N799901) (Bulankova et al., 2013), *CYCB2;4::GUS* (N799902) (Bulankova et al., 2013), *CYCB3;1::GUS* (N799903) (Bulankova et al., 2013) were in the Col-0 background, with the exception of *CYC-D3;1::GUS* which was in Ler-0 background.

Generation of transgenic plants

The *spt-13*^{ge} CRISPR mutant was obtained as follows: Two guides were designed flanking the SPT amphipathic helix on the SPT first intron (Groszmann et al., 2008). The guides were amplified, including the classic Extension-Flip (EF) backbone (Castel et al., 2018; Chen et al., 2013) and BsaI restriction sites, to be compatible with the "Golden Gate" cloning method (Engler et al., 2014). The cloning and CRISPR design followed that detailed in Castel et al. (2018) (Engler et al., 2014), the primers for the sgRNA amplification included the BsaI restriction sites associated with Golden Gate compatible overhangs and are listed below. The reverse sequence corresponds to sgRNA_t192 from (Castel et al., 2018). The amplicons were assembled in level 1 position 3 (pICH47751) with the U6-26 promoter (pICSL90002) using the 'Golden Gate' protocol and a BsaI-HF enzyme (Engler et al., 2014).

The Cas9 expression cassette used was plant codon-optimized and the transcription was driven by the YAO promoter (Li et al., 2013; Yan et al., 2015). The Cas9 was oriented within the construct in the reverse orientation compared to the sgRNAs, as this has been shown to increase CRISPR efficiency. The expression cassette is described in Castel et al. (2018) and corresponds to 'YAO:Cas9_3:E9' in the reverse direction in Castel et al. (2018). The Cas9 expression cassette and a sgRNA expression cassette were assembled in Level 2 pICSL4723 (Castel et al., 2018). In L2, FAST-Red (Shimada et al., 2010) was used as a positive selection marker in plants. The CRISPR construct was dipped in the *35S::GFP-TUA6 x DR5::RFP* line. The T1 seeds were selected for FAST-Red using a Leica M205 microscope. The SPT locus was eventually screened for the mutation (in the T1 generation) by PCR using the SPT Crispr screening primers listed below and by sequencing using the same primers. The T2 generations were screened using sequencing and phenotyping (i.e., radial vs bilateral style). The mutant recovered in this study contained two single nucleotide insertions, one in the region of either sgRNA, resulting in a frame shift and a stop codon after 256 bases from the ATG (Figure S3).

Primers used to amplify the sgRNA cassette:

SPT sgRNA 1 tgtggtctcaATTGCATAAGCACAGAATCTGA CGGGTTTAAGAGCTATGCTGGAA

SPT sgRNA 2 tgtggtctcaATTGTGATACGAGTATCGTAAACCG GTTTAAGAGCTATGCTGGAA

sgRNA rev tgtggtctcaAGCGACCCCAGAAATTGAAC

SPT Crispr_fwd GAAGCAGAGAGTGATGGGAG

SPT Crispr _Rev ATCTGTCTCGTTGCCACTAG

The *35S::SPT–3xFLAG* line was constructed as follows: The full-length coding sequences of SPT were amplified using gene-specific primers listed below, and the PCR products were digested with SifI (NEB) and cloned into the empty pCambia1305–35S::3xFLAG vector, which was pre-digested with DraIII (NEB). The construct was verified by sequencing and introduced into the *Agrobacterium tumefaciens* GV3101 strain and transformed in a

Col-0 background. Transgenic plants were selected on Murashige and Skoog plates supplied with 15 mg /Litre Basta (Sigma).

SPT-F (SfiI) CGCGGATCCGGCCGTCAAGGCCATGATATCACA GAGAGAAGAAAGAGAAG

SPT-R (SfiI) CGCGAATTCGGCCCATGAGGCCAAGTAATTCGA TCTTTTAGGTCAGGTTG

Sample preparation and SEM imaging

Whole inflorescences were fixed in FAA solution (3.7% formaldehyde, 5% glacial acetic acid, 50% ethanol), vacuum infiltrated for 10 min, and gently rocked at room temperature overnight, as previously described (Tsuge et al., 1996). Samples were subsequently dehydrated through an ethanol series (70 to 100%) and critical point-dried using the Leica EM CPD300. Gynoecia were dissected and mounted on a 3.2 × 8 mm pin stub (Agar Scientific). After gold coating, samples were examined using a Zeiss Supra 55VP Field Emission Scanning Electron Microscope using an acceleration voltage of 3 kV.

Sample preparation for calcofluor staining and confocal imaging for MorphoGraphX analysis

Formaldehyde-glutaraldehyde fixation

To preserve the cellular structure, Col, *spt*, and *spt ind* inflorescences were fixed by using a 4% formaldehyde, 1% glutaraldehyde, and 0.5% Triton in 1× Phosphate Buffer Saline (PBS) solution, under vacuum for 2 h (Karnovsky, 1964). Samples were washed twice in 1x PBS buffer.

ClearSee chlorophyll clearing treatment

Chlorophyll autofluorescence was cleared from fixed samples by using Clearsee solution (Kurihara et al., 2015). The solution was prepared using xylitol (final 10% w/v, Sigma), sodium deoxycholate (final 15% w/v, Sigma), and urea (final 25% w/v, Sigma) in water. After fixation and washing, the solution was swapped for Clearsee. The solution was changed every other day for a week or until samples became completely clear.

Stage-9 gynoecia were dissected and placed on glass microscope slides for confocal imaging. Spacers were placed between the slide and coverslip to prevent sample crushing. Samples were imaged using a Zeiss LSM 880 confocal microscope with an air objective (×40/0.6). Calcofluor white was imaged with 405 nm excitation and detection at 425–475 nm. The fluorescence signal was projected into a mesh, and cells were segmented with MGX (de Reuille et al., 2015; Strauss et al., 2022).

The orientation of the cell division plane relative to the organ's overall shape was determined by manually aligning a Bezier surface to the sample and then using the Bezier coordinates to determine organ-centric directions. This method enabled the definition of the division plane's orientation relative to organ directions, thereby providing a context-sensitive framework for analysis. In plant tissues exhibiting strongly anisotropic growth, the configuration of daughter cells post-division was deduced by examining the arrangement of cells in straight lines, known as cell files, and the thickness of their cell walls was assessed, which together indicated how cells typically divide and align (Bencivenga et al., 2016). The orientation of these files provided clues about the direction of the original cell division; cells aligned in a line implied the division occurred at an angle perpendicular to this line. Moreover, new cell walls formed during division were initially thinner than the older, surrounding walls. This contrast in wall thickness was a key indicator for identifying recent cell divisions. Newly formed cell walls are straight immediately following division. Over time, however, the areas of the cell adjacent to these walls exhibit pinching, a process where the cell constricts near the wall, leading to a more pronounced curvature at these locations. The pinching effect could be due to the subsequent cellular growth and mechanical forces acting on the cells after the initial division, resulting in a morphological adaptation. By analyzing the orientation of the cell files and the relative thickness of the cell walls, along with the absence of pinched morphologies near the newly formed walls, the specific locations and configurations of newly formed daughter cells were identified. The pre-division state of cells was virtually reconstructed by fusing inferred daughter cells, effectively simulating an earlier developmental stage. This allowed for an assessment of cells as they would have appeared before division. Thus, the orientation of the virtually reconstructed pre-division cells was compared to their post-division configuration, and the division plane angle was determined.

Confocal analysis

Stage 9 gynoecia were dissected from *35S::GFP-TUA-6* × *DR5::RFP* flowers in the Col-0 and $spt^{ge\text{-}1}$ backgrounds, under a stereomicroscope (Leica M205FA). Samples with a droplet of water were placed on a slide with spacer tape (Grace Bio-Labs SecureSeal™ imaging spacer tape, thickness 0.12 mm) and with a cover slip (thickness #1.5). The images were acquired either using a Zeiss 880 confocal microscope equipped with an Airyscan detector (Huff, 2015) or the Zeiss 780 confocal microscope and imaged using a 40x water immersion objective. Excitation wave lengths were 488 nm and 561 nm. A Z-stack with an interval of 0.12 nm (Zeiss 780) or the optimal was taken when a cell at the gynoecium apex with *DR5::RFP* signal was dividing in WT or, in a $spt^{ge\text{-}1}$ background, a Z-stack was taken if there was a dividing cell at the apical-medial region as *DR5::RFP* signal is genetically absent (Moubayidin & Østergaard, 2014). A water immersion objective with a 40× magnification was used for both microscopes. The Zeiss 780 configuration was set to image GFP and RFP emissions simultaneously with the *DR5::RFP* signal being collected on the sensitive GaAsP spectral detector, as its signal was less clear than that of the *35S::GFP-TUA6*. The samples imaged using the Zeiss 880 images were obtained using the Airyscan detector, in a Z stack using the optimal interval, resolution, and pinhole size suggested for Airyscan processing (ZEISS Zen Black). The Z-stack was deconvoluted using Huygens software when taken on the Zeiss 780. The Airyscan detector was used for the Zeiss 880 (Huff, 2015), which drastically reduced the imaging time and the laser power needed, thus decreasing the photobleaching that occurred when imaging the *DR5::RFP* fluorophore, which was particularly prone to bleaching. Airyscan processing (a form of linear deconvolution) was used to increase the resolution and the file size.

Confocal images were processed using MGX (Strauss et al., 2022). A mesh representative of the 3D surface was extracted from the confocal image stacks, the cells segmented, and the microtubule signal was projected onto the mesh. The orientation of the microtubules was measured on selected samples using "Mesh/Cell Axis/Fibril Orientations," which is based on the FibrilTool plugin in FIJI (Boudaoud et al., 2014).

Confocal analysis of the triple-cell cycle marker and nuclei analysis was carried out as follows: Floral buds of plants harboring the PlaCCI in WT (Desvoyes et al., 2020) and *spt-12* mutant background (Desvoyes et al., 2020) were dissected using a stereomicroscope (Leica S9D), and young gynoecia were mounted in water along their longitudinal axis. Confocal microscopy images

were acquired using the Zeiss LSM880 microscope with 20× water immersion lens. The scanning microscope was used with the following conditions: CFP, excitation at 458 nm and emission from 463 to 510 nm; YFP, excitation at 514 nm and emission from 525 to 560 nm; and RFP, excitation at 561 nm and emission from 570 to 620 nm. Images of samples within an experiment were taken with identical settings. Quantification of fluorescent signals defining cell cycle phases was carried out as follows: Cell cycle phases were primarily defined on the basis of the fluorescent signal of each marker protein scored for individual cells using a combination of FIJI and Zeiss Zen 2011 (black edition) image analysis software to analyze the images. The values for mean intensity signals were then processed accordingly.

All the above confocal analyses have been carried out in the L1 layer (abaxial epidermis).

GUS staining and optical microscope

To visualize the *in vivo* CYCs::GUS expression, inflorescence samples were incubated in 1 mg/mL of ß-glucoronidase substrate X-Gluc (5-bromo-4-chloro-3-indolyl glucuronide, MELFORD) dissolved in Dimethyl sulfoxide (DMSO) and buffer solution (0.1 M Sodium Phosphate Buffer, 0.5 mM K3[Fe(CN)6] + 3 mM K4[Fe (CN)6] 10 mM EDTA, 0. 1% Triton). Samples were vacuum infiltrated for 10 min and incubated at 37°C overnight. Following staining, the reaction buffer was substituted with 70% ethanol until chlorophyll was thoroughly eliminated from the samples. Gynoecium were dissected, mounted in a Chlorohydrate (Sigma) solution, and subjected to analysis using Leica DM600 light microscopy. Images were taken using Leica LAS AF7000 software.

DNA extraction and genotyping

Plant DNA was obtained via modification based on the Edwards' quick DNA extraction protocol for Arabidopsis. Either a young leaf or an inflorescence was crushed using a plastic pestle in a 1.5-ml Eppendorf containing 200 μl of the extraction buffer (200 mM Tris HCL pH7.5, 250 mM NaCl, 25 mM EDTA, 0.5% SDS). The samples were vortexed for 5 sec and then centrifuged at 13 000 rpm for 5 min. One hundred and fifty microliters of the supernatant was added to a 1.5 ml Eppendorf containing 150 μl of isopropanol. The samples were then vortexed for 5 sec and let to react at room temperature for 10 min, followed by centrifugation at 13 000 rpm for 10 min. The supernatant was poured off, and the pellet was dried for half an hour. The dry DNA was resuspended in 50 μl of H_20 and stored at 4°C.

The CYC-D1;1 WT allele and the *cyc-d1;1* gabi mutant insertion (Masubelele et al., 2005) were identified using the following primer pairs: CYC-D1;1 WT (CYC-D1;1gabi F + CYC-D1;1gabi R) and *cyc-d1;1* gabi mutant (CYC-D1;1gabi F + o8474):

CYC-D1;1gabi F: 5′ATTCATGGCCTGGTGATTCTATC3′

CYC-D1;1gaby R: 5′TTACAAAGTTTTCAATAAAGCCGA3′

o8474: 5′ATAATAACGCTGCGGACATCTACATTTT3′

The *cyc-d3;3* Ds insertion (Dewitte et al., 2007) as identified using the following primer pair: CYC-D3;3 CYC-D3;3 R + Ds5-1:

CYC-D3;3 R: 5′GCTGAGATTGGTATACAGCTTCGTG3′.

Ds5-1: 5′ACGGTCGGGAAACTAGCTCTA3′.

The SPT WT allele and the *spt-12* T-DNA insertion (Ichihashi et al., 2010) were identified using the following primer pairs: SPT WT (SPT WT F + SPT WT R) and spt-12 mutant (SPT WT F + p745):

SPT WT F: 5′GAAGAAGCAGAGAGTGATGGGAGA3′.

SPT WT R: 5′TGACTTGGAAGAGGGAGCTTCA3′.

p745: 5′AACGTCCGCAATGTGTTATTAAGTTGTC3′

ChIP assays, RNA extraction, cDNA synthesis, and qRT-PCR experiments

For ChIP experiments and *in vitro* expression analysis, treatments of *35S*::*IND*:*GR* seedlings with or without Dexamethasone (Dex) (Sigma, D1756) and Indole-3-Acetic Acid (IAA) (Sigma, I2886) were performed as previously described (Ichihashi et al., 2010). In brief, 7-day-old *35S*::*IND*:*GR* seedlings, grown in MS liquid under constant light and gentle shaking conditions, were treated with either of the following: 10 μM Dexamethasone (Dex) (Sigma, D1756) solution for 24 h; 50 μM IAA solution for 3 h; a combination of both DEX and IAA; or equivalent concentrations of corresponding solvents (DMSO for DEX treatments and/or 70% ethanol for IAA treatments) as mock. Similarly, 7-day-old *35S*::*SPT-FLAG* and Col-0 seedlings were grown in MS liquid prior to RNA extraction.

For *in vitro* expression analysis in loss-of-function and over-expressing SPT backgrounds, young inflorescences of Col-0, *spt-12* and three independent lines of *35S*::*SPT-FLAG* were used for RNA extraction.

Total RNA was extracted using the RNeasy Plant mini kit (Quiagen), and cDNAs synthesis was obtained with M-MLV Reverse Transcriptase (Promega) according to the manufacturer's instructions, as previously reported (Moubayidin & Østergaard, 2014). Gene-specific expression levels were obtained via qRT-PCR experiments, calculated relative to *UBIQUITIN 10* using the $2^{-\Delta\Delta ct}$ method. Statistical analysis was done in MS Excel (ANOVA: Single Factor) using $P < 0.05$. Primers were designed according to the recommendations of Applied Biosystems. Quantitative RT-PCR (qRT-PCR) analysis was conducted using the gene-specific primers listed below:

Ub10 L GGCCTTGTATAATCCCTGATGAATAAG

Ub10 R AAAGAGATAACAGGAACGGAAACATAGT

CYC-D1;1 RT 3′UTR fwd GGTTTTGGGGTTGGTTGGTT

CYC-D1;1 RT 3′UTR rev CGCTCCCCTGTCTTATCCAT

CYC-D1;1 5′UTR RT GGAGATGAATCAAACCGGAGC

CYC-D1;1 5′UTR RT ACCTTCACTCTTCTCTCCACA

The following primer sequences are from (Jiang et al., 2024).

SPT Fwd: GATTCGACCCCCTGAAGCAA

SPT Rev: TTCCCGACTCATCTCCACG

The following primer sequences are from (Forzani et al., 2014).

ChIPCyc-D3;3_-1750 bp
CTAATGGAACATATTGTAGACCTATTTGG

ChIPCyc-D3;3_-1750 bp
AACAAAGAAATTCCTTATCATATCGCT

ChIPCyc-D3;3_-700 bp
ACACAATGACAGTGACTCTACACATTACG

ChIPCyc-D3;3_-700 bp
CGTCATTAGTACTTTGATTTTGGTTAATACAAC

ChIPCyc-D3;3_5UTR AGAGGACAAGCGTGAAATAAAACCCT

ChIPCyc-D3;3_5UTR CTCTGGATTCTTCACTCTGTGTGAGA

Statistical analysis

The study of division plane orientation used Analysis of Variance (ANOVA) to assess angle differences in gynoecia at two developmental stages (stages 9 and 12). For stage 9, 154 divisions and 3 biological replicates per line were analyzed. ANOVA ($F(2, 158) = 145.3$, $P < 0.001$) followed by Tukey HSD revealed no significant difference between WT style and WT replum ($P = 0.808$), but

significant differences between *spt ind* style and WT replum, and *spt ind* style and WT style (both $P < 0.001$). At stage 12, 58 divisions and 3 biological replicates per line were examined. ANOVA ($F(2, 58) = 354.3$, $P < 0.001$) followed by Tukey HSD indicated no significant difference between WT style and WT replum ($P = 0.651$), but significant differences were observed between *spt* style and WT replum and *spt* style and WT style (both $P < 0.001$).

The statistical analyses of the PlaCCI reporter were performed in GraphPad Prism software, version 8.2.1. Specific statistical test used is indicated in the figure legend and were always two-tailed.

AUTHOR CONTRIBUTIONS

Conceptualization, LM; methodology, BT-B, SHK, KAM, IJ, NT, YJ, and LM; software, NT and RSS; formal analysis, BT-B, SHK, KAM, IJ, NT, YJ, MM, RSS, and LM; investigation, BT-B, SHK, KAM, IJ, NT, YJ, and LM; data curation, BT-B, SHK, KAM, IJ, NT, YJ, and LM; writing—original draft preparation, LM; writing—review and editing, BT-B, SHK, KAM, IJ, NT, YJ, RSS, and LM; supervision, RSS and LM; project administration, LM; funding acquisition, LM. All authors have read and agreed to the published version of the manuscript.

ACKNOWLEDGMENTS

We thank Prof. Crisanto Gutierrez (Centro de Biología Molecular Severo Ochoa) and Dr. Jordi Chan (John Innes Centre) for sharing the PlaCCI and *TUA6:GFP* lines, respectively; Prof. James Murray (Cardiff University) for sharing *cyc-d1;1*, *cyc-d1;1 cyc-d3;3*, *CYC-D1;1::GUS*, *CYC-D3;1::GUS*, *CYC-D3;2::GUS*, *CYC-D3;3::GUS*, *CYC-D4;2::GUS*, *CYC-D5;1::GUS*, *CYC-D6;1::GUS*, *CYC-D7;1::GUS* lines; Prof. Lars Østergaard (John Innes Centre) and Dr. Karim Sorefan (Sheffield University) for sharing unpublished data; Prof. Jonathan Jones (The Sainsbury Lab) and Dr. Silvia Costa (John Innes Centre) for early discussions. We also thank Dr. Pauline Stephenson and Dr. Benguo Gu (John Innes Centre) and Prof Pingtao Ding (Leiden University) for technical support.

FUNDING INFORMATION

This research was funded by the Royal Society University Research Fellowship URF\R1\180091 (LM), the Royal Society Enhanced Research Expenses RF\ERE\210323 (LM), the Royal Society Research Fellows Enhancement Awards RGF \EA\181077 (LM), the John Innes Foundation (NT), the Biotechnology and Biological Sciences Research Council NRP Doctoral Training Programme Studentship BB/T008717/1 (KAM), and the Institute Strategic Programme grant (BB/X01102X/1) to the John Innes Centre from the Biotechnology and Biological Sciences Research Council.

CONFLICT OF INTEREST STATEMENT

The authors declare no conflict of interest. The funders had no role in the design of the study; in the collection, analyses, or interpretation of data; in the writing of the manuscript; or in the decision to publish the results.

DATA AVAILABILITY STATEMENT

All data needed to evaluate the conclusions in this paper are present in the paper and/or the Supplementary Materials. All new genetic material (high-order mutants, transgenic lines) will be made available to the scientific community upon request and with no limitation by contacting the corresponding author.

SUPPORTING INFORMATION

Additional Supporting Information may be found in the online version of this article.

Figure S1. Auxin accumulation correlates with cell-division plane orientation in the medial-apical domain of developing radial and bilateral gynoecium apices

Figure S2. Characterization of the CRISPR-CAS9 *spt-13^{ge}* mutant

Figure S3. GUS-fused transcriptional analysis of cyclin expression during gynoecium development

Figure S4. Molecular control of CYC-Ds by SPT and characterization of *35S::SPY-FLAG* lines.

REFERENCES

Alon, U. (2007) Network motifs: theory and experimental approaches. *Nature Reviews Genetics*, **8**, 450–461.

Bencivenga, S., **Serrano-Mislata, A.**, **Bush, M.**, **Fox, S.** & **Sablowski, R.** (2016) Control of oriented tissue growth through repression of organ boundary genes promotes stem morphogenesis. *Developmental Cell*, **39**, 198–208.

Boer, D.R., **Freire-Rios, A.**, **van den Berg, W.A.M.**, **Saaki, T.**, **Manfield, I.W.**, **Kepinski, S.** ***et al.*** (2014) Structural basis for DNA binding specificity by the auxin-dependent ARF transcription factors. *Cell*, **156**, 577–589.

Boudaoud, A., **Burian, A.**, **Borowska-Wykręt, D.**, **Uyttewaal, M.**, **Wrzalik, R.**, **Kwiatkowska, D.** ***et al.*** (2014) FibrilTool, an ImageJ plug-in to quantify fibrillar structures in raw microscopy images. *Nature Protocols*, **9**, 457–463.

Bulankova, P., **Akimcheva, S.**, **Fellner, N.** & **Riha, K.** (2013) Identification of Arabidopsis meiotic cyclins reveals functional diversification among plant cyclin genes. *PLoS Genetics*, **9**, e1003508.

Carabelli, M., **Turchi, L.**, **Morelli, G.**, **Østergaard, L.**, **Ruberti, I.** & **Moubayidin, L.** (2021) Coordination of biradial-to-radial symmetry and tissue polarity by HD-ZIP II proteins. *Nature Communications*, **12**, 4321.

Castel, B., **Tomlinson, L.**, **Locci, F.**, **Yang, Y.** & **Jones, J.D.G.** (2018) Optimization of T-DNA architecture for Cas9-mediated mutagenesis in Arabidopsis. *PLoS One*, **14**, 1–20.

Chakrabortty, B., **Willemsen, V.**, **Zeeuw, T.d.**, **Liao, C.Y.**, **Weijers, D.**, **Mulder, B.** ***et al.*** (2018) A plausible microtubule-based mechanism for cell division orientation in plant embryogenesis. *Current Biology*, **28**, 3031–3043.

Chen, B., **Gilbert, L.A.**, **Cimini, B.A.**, **Schnitzbauer, J.**, **Zhang, W.**, **Li, G.W.** ***et al.*** (2013) Dynamic imaging of genomic loci in living human cells by an optimized CRISPR/Cas system. *Cell*, **155**, 1479–1491.

Collins, C., **Dewitte, W.** & **Murray, J.A.H.** (2012) D-type cyclins control cell division and developmental rate during Arabidopsis seed development. *Journal of Experimental Botany*, **63**, 3571–3586.

Costa, S. (2017) Are division plane determination and cell-cycle progression coordinated? *New Phytologist*, **213**, 16–21.

Cruz-Ramírez, A., **Díaz-Triviño, S.**, **Blilou, I.**, **Grieneisen, V.A.**, **Sozzani, R.**, **Zamioudis, C.** ***et al.*** (2012) A Bistable circuit involving SCARECROW-RETINOBLASTOMA integrates cues to inform asymmetric stem cell division. *Cell*, **150**, 1002–1015.

D'Ario, M., **Tavares, R.**, **Schiessl, K.**, **Desvoyes, B.**, **Gutierrez, C.**, **Howard, M.** ***et al.*** (2021) Cell size controlled in plants using DNA content as an internal scale. *Science*, **372**, 1176–1181.

Davison, A., **McDowell, G.S.**, **Holden, J.M.**, **Johnson, H.F.**, **Koutsovoulos, G.D.**, **Liu, M.M.** ***et al.*** (2016) Formin is associated with left-right asymmetry in the pond snail and the frog. *Current Biology*, **26**, 654–660.

de Reuille, P.B., **Routier-Kierzkowska, A.L.**, **Kierzkowski, D.**, **Basse, G.W.**, **Schüpbach, T.**, **Tauriello, G. *et al.*** (2015) MorphoGraphX: a platform for quantifying morphogenesis in 4D. *eLife*, **4**, 1–20.

De Rybel, B., **Möller, B.**, **Yoshida, S.**, **Grabowicz, I.**, **Barbier de Reuille, P.**, **Boeren, S. *et al.*** (2013) A bHLH complex controls embryonic vascular tissue establishment and indeterminate growth in Arabidopsis. *Developmental Cell*, **24**, 426–437.

Dello Ioio, R., **Nakamura, K.**, **Moubayidin, L.**, **Perilli, S.**, **Taniguchi, M.**, **Morita, T. *et al.*** (2008) A genetic framework for genetic control of cell division and differentiation in the root meristem. *Science*, **1979**, 1543–1547.

Desvoyes, B., **Arana-Echarri, A.**, **Barea, M.D.** & **Gutierrez, C.** (2020) A comprehensive fluorescent sensor for spatiotemporal cell cycle analysis in Arabidopsis. *Nature Plants*, **6**, 1330–1334.

Dewitte, W., **Scofield, S.**, **Alcasabas, A.A.**, **Maughan, S.C.**, **Menges, M.**, **Braun, N. *et al.*** (2007) Arabidopsis CYCD3 D-type cyclins link cell proliferation and endocycles and are rate-limiting for cytokinin responses. *Proceedings of the National Academy of Sciences USA*, **104**, 14537–14542.

Eldridge, T., **Łangowski, Ł.**, **Stacey, N.**, **Jantzen, F.**, **Moubayidin, L.**, **Sicard, A. *et al.*** (2016) Fruit shape diversity in the Brassicaceae is generated by varying patterns of anisotropy. *Development*, **143**, 3394–3406.

Engler, C., **Youles, M.**, **Gruetzner, R.**, **Ehnert, T.-M.**, **Werner, S.**, **Jones, J.D.G. *et al.*** (2014) A Golden Gate modular cloning toolbox for plants. *ACS Synthetic Biology*, **3**, 839–843.

Erzberger, A., **Jacobo, A.**, **Dasgupta, A.** & **Hudspeth, A.J.** (2020) Mechanochemical symmetry breaking during morphogenesis of lateral-line sensory organs. *Nature Physics*, **16**, 949–957.

Facette, M.R., **Rasmussen, C.G.** & **Van Norman, J.M.** (2018) A plane choice : coordinating timing and orientation of cell division during plant development. *Current Opinion in Plant Biology*, **47**, 47–55.

Forzani, C., **Aichinger, E.**, **Sornay, E.**, **Willemsen, V.**, **Laux, T.**, **Dewitte, W. *et al.*** (2014) WOX5 suppresses CYCLIN D activity to establish quiescence at the center of the root stem cell niche. *Current Biology*, **24**, 1939–1944.

Friml, J., **Yang, X.**, **Michniewicz, M.**, **Weijers, D.**, **Quint, A.**, **Tietz, O. *et al.*** (2004) (2004) a PINOID-dependent binary switch in apical-basal PIN polar targeting directs auxin efflux. *Science*, **306**, 862–865.

Genikhovich, G. & **Technau, U.** (2017) On the evolution of bilaterality. *Development*, **144**, 3392–3404.

Girin, T., **Paicu, T.**, **Stephenson, P.**, **Fuentes, S.**, **Körner, E.**, **O'Brien, M. *et al.*** (2011) INDEHISCENT and SPATULA interact to specify carpel and valve margin tissue and thus promote seed dispersal in Arabidopsis. *Plant Cell*, **23**, 3641–3653.

Girin, T., **Sorefan, K.** & **Østergaard, L.** (2009) Meristematic sculpting in fruit development. *Journal of Experimental Botany*, **60**, 1493–1502.

Girin, T., **Stephenson, P.**, **Goldsack, C.M.P.**, **Kempin, S.A.**, **Perez, A.**, **Pires, N. *et al.*** (2010) Brassicaceae INDEHISCENT genes specify valve margin cell fate and repress replum formation. *Plant Journal*, **63**, 329–338.

Goentoro, L., **Shoval, O.**, **Kirschner, M.W.** & **Alon, U.** (2009) The incoherent feedforward loop can provide fold-change detection in gene regulation. *Molecular Cell*, **36**, 894–899.

Gómez-Felipe, A., **Branchini, E.**, **Wang, B.**, **Marconi, M.**, **Bertrand-Rakusová, H.**, **Stan, T. *et al.*** (2024) Two orthogonal differentiation gradients locally coordinate fruit morphogenesis. *Nature Communications*, **15**, 2912.

Groszmann, M., **Bylstra, Y.**, **Lampugnani, E.R.** & **Smyth, D.R.** (2010) Regulation of tissue-specific expression of SPATULA, a bHLH gene involved in carpel development, seedling germination, and lateral organ growth in Arabidopsis. *Journal of Experimental Botany*, **61**, 1495–1508.

Groszmann, M., **Paicu, T.**, **Alvarez, J.P.**, **Swain, S.M.** & **Smyth, D.R.** (2011) SPATULA and ALCATRAZ, are partially redundant, functionally diverging bHLH genes required for Arabidopsis gynoecium and fruit development. *Plant Journal*, **68**, 816–829.

Groszmann, M., **Paicu, T.** & **Smyth, D.R.** (2008) Functional domains of SPATULA, a bHLH transcription factor involved in carpel and fruit development in Arabidopsis. *Plant Journal*, **55**, 40–52.

Guilfoyle, T.J. (2015) The PB1 domain in auxin response factor and aux/IAA proteins: a versatile protein interaction module in the auxin response. *Plant Cell*, **27**, 33–43.

Gutierrez, C. (2009) The Arabidopsis cell division cycle. *The Arabidopsis Book*, **7**, 1–19.

Han, S.K., **Herrmann, A.**, **Yang, J.**, **Iwasaki, R.**, **Sakamoto, T.**, **Desvoyes, B. *et al.*** (2022) Deceleration of the cell cycle underpins a switch from proliferative to terminal divisions in plant stomatal lineage. *Developmental Cell*, **57**, 569–582.

Hartman, K.S. & **Muroyama, A.** (2023) Polarizing to the challenge: new insights into polarity-mediated division orientation in plant development. *Current Opinion in Plant Biology*, **74**, 102383.

Heisler, M.G., **Atkinson, a.**, **Bylstra, Y.H.**, **Walsh, R.** & **Smyth, D.R.** (2001) SPATULA, a gene that controls development of carpel margin tissues in Arabidopsis, encodes a bHLH protein. *Development*, **128**, 1089–1098.

Herth, W. & **Schnepf, E.** (1980) The fluorochrome, calcofluor white, binds oriented to structural polysaccharide fibrils. *Protoplasma*, **105**, 129–133.

Huff, J. (2015) The Airyscan detector from ZEISS: confocal imaging with improved signal-to-noise ratio and super-resolution. *Nature Methods*, **12**, 1–2.

Ichihashi, Y., **Horiguchi, G.**, **Gleissberg, S.** & **Tsukaya, H.** (2010) The bHLH transcription factor SPATULA controls final leaf size in arabidopsis thaliana. *Plant & Cell Physiology*, **51**, 252–261.

Imai, K.K., **Ohashi, Y.**, **Tsuge, T.**, **Yoshizumi, T.**, **Matsui, M.**, **Oka, A. *et al.*** (2006) The A-type cyclin CYCA2;3 is a key regulator of ploidy levels in Arabidopsis endoreduplication. *Plant Cell*, **18**, 382–396.

Jiang, Y., **Curran-French, S.**, **Koh, S.W.H.**, **Jamil, I.**, **Gu, B.**, **Argirò, L. *et al.*** (2024) O-glycosylation of the transcription factor SPATULA promotes style development in Arabidopsis. *Nature Plants*, **10**, 283–299.

Karnovsky, M.J. (1964) A Formaldehyde-Glutaraldehyde Fixative of High Osmolality for Use in Electron Microscopy. https://www.researchgate.net/publication/244955881

Kuhn, A., **Ramans Harborough, S.**, **McLaughlin, H.M.**, **Natarajan, B.**, **Verstraeten, I.**, **Friml, J. *et al.*** (2020) Direct ETTIN-auxin interaction controls chromatin states in gynoecium development. *eLife*, **9**, 863134.

Kurihara, D., **Mizuta, Y.**, **Sato, Y.** & **Higashiyama, T.** (2015) ClearSee: a rapid optical clearing reagent for whole-plant fluorescence imaging. *Development*, **142**, 4168–4179.

Ie, J., **Liu, X.G.**, **Yang, K.Z.**, **Chen, X.L.**, **Zou, J.J.**, **Wang, H.Z. *et al.*** (2014) Auxin transport and activity regulate stomatal patterning and development. *Nature Communications*, **5**, 1–8.

Li, J.-F., **Norville, J.E.**, **Aach, J.**, **McCormack, M.**, **Zhang, D.**, **Bush, J. *et al.*** (2013) Multiplex and homologous recombination–mediated genome editing in Arabidopsis and Nicotiana benthamiana using guide RNA and Cas9. *Nature Biotechnology*, **31**, 688–691.

Li, X.-M., **Jenke, H.**, **Strauss, S.**, **Bazakos, C.**, **Mosca, G.**, **Lymbouridou, R. *et al.*** (2024) Cell-cycle-linked growth reprogramming encodes developmental time into leaf morphogenesis. *Current Biology*, **34**, 541–556.

Liljegren, S.J., **Roeder, A.H.K.**, **Kempin, S.A.**, **Gremski, K.**, **Østergaard, L.**, **Guimil, S. *et al.*** (2004) Control of fruit patterning in Arabidopsis by INDEHISCENT. *Cell*, **116**, 843–853.

MacAlister, C.A., **Ohashi-Ito, K.** & **Bergmann, D.C.** (2007) Transcription factor control of asymmetric cell divisions that establish the stomatal lineage. *Nature*, **445**, 537–540.

Makkena, S. & **Lamb, R.S.** (2013) The bHLH transcription factor SPATULA regulates root growth by controlling the size of the root meristem. *BMC Plant Biology*, **1**, 13.

Mangan, S. & **Alon, U.** (2003) Structure and function of the feed-forward loop network motif. *Proceedings of the National Academy of Sciences*, **100**, 11980–11985.

Marhavý, P., **Bielach, A.**, **Abas, L.**, **Abuzeineh, A.**, **Duclercq, J.**, **Tanaka, H. *et al.*** (2011) Cytokinin modulates endocytic trafficking of PIN1 auxin efflux carrier to control plant organogenesis. *Developmental Cell*, **21**, 796–804.

Marin, E., **Jouannet, V.**, **Herz, A.**, **Lokerse, A.S.**, **Weijers, D.**, **Vaucheret, H. *et al.*** (2010) miR390, Arabidopsis TAS3 tasiRNAs, and their AUXIN RESPONSE FACTOR targets define an autoregulatory network quantitatively regulating lateral root growth. *Plant Cell*, **22**, 1104–1117.

Masubelele, N.H., **Dewitte, W.**, **Menges, M.**, **Maughan, S.**, **Collins, C.**, **Huntley, R. *et al.*** (2005) D-type cyclins activate division in the root apex to promote seed germination in Arabidopsis. Proceedings of the National Academy of Sciences, 102, 15694-15699.

Menges, M., **Samland, A.K.**, **Planchais, S.** & **Murray, J.A.H.** (2006) The D-type cyclin CYCD3;1 is limiting for the G1-to-S-phase transition in Arabidopsis. *Plant Cell*, **18**, 893–906.

Moubayidin, L., **Di Mambro, R.** & **Sabatini, S.** (2009) Cytokinin-auxin crosstalk. *Trends in Plant Science*, **14**, 557–562.

Moubayidin, L. & **Østergaard, L.** (2014) Dynamic control of auxin distribution imposes a bilateral-to-radial symmetry switch during gynoecium development. *Current Biology*, **24**, 2743–2748.

Moubayidin, L. & **Østergaard, L.** (2015) Symmetry matters. *New Phytologist*, **207**, 985–990.

Moubayidin, L., **Salvi, E.**, **Giustini, L.**, **Terpstra, I.**, **Heidstra, R.**, **Costantino, P.** ***et al.*** (2016) A SCARECROW-based regulatory circuit controls Arabidopsis thaliana meristem size from the root endodermis. *Planta*, **243**, 1159–1168.

Müller, C.J., **Larsson, E.**, **Spíchal, L.** & **Sundberg, E.** (2017) Cytokinin-auxin crosstalk in the gynoecial primordium ensures correct domain patterning. *Plant Physiology*, **175**, 1144–1157.

Nahar, M.A.U., **Ishida, T.**, **Smyth, D.R.**, **Tasaka, M.** & **Aida, M.** (2012) Interactions of CUP-SHAPED COTYLEDON and SPATULA genes control carpel margin development in arabidopsis thaliana. *Plant & Cell Physiology*, **53**, 1134–1143.

Oakenfull, E.A., **Riou-Khamlichi, C.** & **Murray, J.A.H.** (2002) Plant D-type cyclins and the control of G1 progression. *Philosophical Transactions of the Royal Society, B: Biological Sciences*, **357**, 749–760.

Rasmussen, C.G. & **Bellinger, M.** (2018) An overview of plant division-plane orientation. *New Phytologist*, **219**, 505–512.

Reyes-Olalde, J.I., **Zúñiga-Mayo, V.M.**, **Serwatowska, J.**, **Chavez Montes, R.A.**, **Lozano-Sotomayor, P.**, **Herrera-Ubaldo, H.** ***et al.*** (2017) The bHLH transcription factor SPATULA enables cytokinin signaling, and both activate auxin biosynthesis and transport genes at the medial domain of the gynoecium. *PLoS Genetics*, **13**, e1006726.

Sabatini, S., **Beis, D.**, **Wolkenfelt, H.**, **Murfett, J.**, **Guilfoyle, T.**, **Malamy, J.** ***et al.*** (1999) An auxin-dependent distal organizer of pattern and polarity in the Arabidopsis root. *Cell*, **99**, 463–472.

Schaefer, E., **Belcram, K.**, **Uyttewaal, M.**, **Duroc, Y.**, **Goussot, M.**, **Legland, D.** ***et al.*** (2017) The preprophase band of microtubules controls the robustness of cell division orientation in plants. *Science*, **189**, 186–189.

Shimada, T.L., **Shimada, T.** & **Hara-Nishimura, I.** (2010) A rapid and non-destructive screenable marker, FAST, for identifying transformed seeds of Arabidopsis thaliana: TECHNICAL ADVANCE. *Plant Journal*, **61**, 519–528.

Simonini, S., **Bemer, M.**, **Bencivenga, S.**, **Gagliardini, V.**, **Pires, N.D.**, **Desvoyes, B.** ***et al.*** (2021) The Polycomb group protein MEDEA controls cell proliferation and embryonic patterning in Arabidopsis. *Developmental Cell*, **56**, 1945–1960.

Simonini, S., **Deb, J.**, **Moubayidin, L.**, **Stephenson, P.**, **Valluru, M.**, **Freire-rios, A.** ***et al.*** (2016) A noncanonical auxin-sensing mechanism is required for organ morphogenesis in Arabidopsis. *Genes & Development*, **30**, 2286–2296.

Sorefan, K., **Girin, T.**, **Liljegren, S.J.**, **Ljung, K.**, **Robles, P.**, **Galván-Ampudia, C.S.** ***et al.*** (2009) A regulated auxin minimum is required for seed dispersal in Arabidopsis. *Nature*, **459**, 583–586.

Sozzani, R., **Cui, H.**, **Moreno-Risueno, M.**, **Busch, W.**, **Van Norman, J.M.**, **Vernoux, T.** ***et al.*** (2010) Spatiotemporal regulation of cell-cycle genes by SHORTROOT links patterning and growth. *Nature*, **466**, 128–132.

Spinner, L., **Gadeyne, A.**, **Belcram, K.**, **Goussot, M.**, **Moison, M.**, **Duroc, Y.** ***et al.*** (2013) A protein phosphatase 2A complex spatially controls plant cell division. *Nature Communications*, **4**, 1863.

Strauss, S., **Runions, A.**, **Lane, B.**, **Eschweiler, D.**, **Bajpai, N.**, **Trozzi, N.** ***et al.*** (2022) Using positional information to provide context for biological image analysis with MorphoGraphX 2.0. *eLife*, **11**, e72601.

Takahashi, I., **Kojima, S.**, **Sakaguchi, N.**, **Umeda-Hara, C.** & **Umeda, M.** (2010) Two Arabidopsis cyclin A3s possess G1 cyclin-like features. *Plant Cell Reports*, **29**, 307–315.

Toledo-Ortiz, G., **Huq, E.** & **Quail, P.H.** (2003) The Arabidopsis basic/helix-loop-helix transcription factor family. *Plant Cell*, **15**, 1749–1770.

Tsuge, T., **Tsukaya, H.** & **Uchimiya, H.** (1996) Two independent and polarized processes of cell elongation regulate leaf blade expansion in *Arabidopsis thaliana* (L.) Heynh. *Development*, **122**, 1589–1600.

Ueda, K., **Matsuyama, T.** & **Hashimoto, T.** (1998) Visualization of microtubules in living cells of transgenic Arabidopsis thaliana. *Protoplasma*, **206**, 201–206.

Winter, C.M., **Szekely, P.**, **Popov, V.**, **Belcher, H.**, **Carter, R.**, **Jones, M.** ***et al.*** (2024) SHR and SCR coordinate root patterning and growth early in the cell cycle. *Nature*, **626**, 611–616.

Yan, L., **Wei, S.**, **Wu, Y.**, **Hu, R.**, **Li, H.**, **Yang, W.** ***et al.*** (2015) High-efficiency genome editing in Arabidopsis using YAO promoter-driven CRISPR/Cas9 system. *Molecular Plant*, **8**, 1820–1823.

Yoshida, S., **BarbierdeReuille, P.**, **Lane, B.**, **Bassel, G.W.**, **Prusinkiewicz, P.**, **Smith, R.S.** ***et al.*** (2014) Genetic control of plant development by overriding a geometric division rule. *Developmental Cell*, **29**, 75–87.

Zhang, Y., **Iakovidis, M.** & **Costa, S.** (2016) Control of patterns of symmetric cell division in the epidermal and cortical tissues of the Arabidopsis root. *Development*, **143**, 978–982.